

1 **Sandstone diagenesis in sediment-lava sequences: Exceptional examples of volcanically driven diagenetic**
2 **compartmentalization in Dune Valley, Huab Outliers, NW Namibia.**

3 Clayton Grove¹, Dougal A. Jerram^{2,3}, Jon G. Gluyas⁴, Richard J. Brown⁴

4 ¹Siccar Point Energy Limited, H1, Hill of Rubislaw, Aberdeen, AB15 6BY

5 ²Centre for Earth Evolution and Dynamics (CEED), University of Oslo, 0316 Oslo, Norway

6 ³DougalEARTH Ltd. Solihull, United Kingdom (www.dougalearth.com)

7 ⁴Department of Earth Sciences, Durham University, DH1 3LE, United Kingdom

8 (E-mail: clayton.grove@siccarpointenergy.co.uk)

9

10

11

ABSTRACT

12

At the base of many flood basalt sequences and along volcanic rifted margins, volcanism can compete with the

13

existing sedimentary environments, resulting in interbedded sequences of volcanic rocks and sediments. Here

14

we report on sediment interlayers that are found in the lowermost volcanic units of the Etendeka flood basalts in

15

NW Namibia (Twyfelfontein/Awahab Formations), part of the much larger Paraná-Etendeka Igneous Province.

16

The sandstone bodies, predominantly eolian dunes, are isolated in a sequence of Lower Cretaceous (~ 134 Ma)

17

lava flows. The upper most part or where sediment deposition and lava emplacement is observed to interact is

18

characterized by barchanoid dunes, which were actively migrating during the emplacement of the lava flows.

19

The fossil (isolated by lava) barchan dunes studied in “Dune Valley” show three characteristically different

20

diagenetic styles. In Dune Valley, each dune body is completely encapsulated by lava, with additional igneous

21

intrusions cutting through some bodies. We recognize three distinct styles of diagenesis: Type 1: Fossilised

22

dunes that are red in color and lack major authigenic mineralization, with grain compaction and subsequent

23

porosity loss being the dominant diagenetic process. Type 2: Dunes that have been bleached white, which have

24

undergone a more complex diagenetic pathway. Type 2 dunes have abundant calcite, kaolinite, and böhmite as

25

authigenic phases and lack hematite grain coatings. Detrital plagioclase is absent in white dunes (XRD analysis),

26

with pseudomorphs of kaolinite common. This diagenetic assemblage results in the white dunes having lower

27

porosity and permeability compared to the red dunes. The observations are probably due to a flux of carbon

28

dioxide (CO₂), hydrogen sulfide (H₂S) and/or hydrogen (H₂) -rich hydrothermal groundwater derived from

29

igneous intrusions below. Type 3: “Hot contact” effects at lava-flow contacts, where the unconsolidated dunes

30

were rapidly indurated during lava emplacement (volcano-eogenesis). Type 3 diagenesis is restricted to << 1 m

31 depth below lava contacts and common in dunes displaying both Type 1 and Type 2 diagenesis. The distribution
32 of diagenetic Types 1 and 2 is dune specific, and throughout Dune Valley approximately half of the dunes have
33 been bleached (e.g. Type 2 diagenesis), whereas diagenetic Type 3 is a hot contact phenomenon and is therefore
34 found along all basal lava and dike contacts. This work has relevance to understanding the development of
35 sediment-lava systems, to hydrocarbon exploration and development in preserved sediment-lava sequences, and
36 the hydrothermal process described provide an example of natural CO₂ sequestration.

37

38

39

INTRODUCTION

40 Sediment-lava interbeds are important as they have the potential to preserve features from paleoenvironments
41 not usually recorded in the rock record, are targets for hydrocarbon exploration in volcanic margins, and provide
42 detailed constraints on paleo-environment and burial effects in volcanism influenced basins. The most common
43 examples of significant sediment-lava interbeds can be found in large-volume lava-flow fields, in volcanic
44 margins, and in continental flood basalts. Sedimentary deposits that are partially or totally buried by volcanic
45 rocks represent a transition or switching between sedimentary and volcanic environments. The eruption of lava
46 flows and/or explosive units has the potential to quickly bury and interact with the sedimentary systems that are
47 present at the time of their emplacement due to the overwhelming volumes of volcanic material erupted in
48 relatively short time intervals (e.g. Peate et al. 2003; Ross et al. 2005; Jerram and Widdowson 2005; Bryan et al.
49 2010). The sedimentary systems present can be engulfed rapidly and preserved almost entirely by the lavas (e.g,
50 Mountney et al. 1999a; Jerram et al. 2000a; Jerram and Stollhofen 2002; Petry et al. 2007). Where active
51 sedimentation is contemporaneous with lava-flow emplacement, interbedded sediments and lava flows can
52 develop. This can result in a complex spatial organization as sediments and lava dynamically interact and
53 compete for accommodation (e.g. Jerram et al. 1999a; Jerram and Stollhofen 2002; Scherer 2002; Waichel et al.
54 2008; Waichel et al. 2011; Schofield and Jolley, 2013). Such mixed volcanic-sedimentary systems favor
55 diagenesis not commonly found elsewhere, such as at hot lava-sediment contacts and authigenesis due to hot
56 hydrothermal groundwater. Additionally, these sequences can be dissected by intrusions associated with the
57 emplacement of the volcanic system, which can act as conduits to flow, modify the permeability system,
58 compartmentalize the basin, and enhance hydrothermal activity (e.g. Schofield et al., 2015; Senger et al., 2017;
59 Angkasa et al., 2017).

60 Offshore petroleum exploration has also highlighted the occurrence of similar isolated sandstone bodies within
61 prospective hydrocarbon exploration areas in volcanic rifted margins worldwide (e.g. Jungslager 1999; Davison
62 1999; Schutter 2003; Smallwood et al. 2004). This raises additional questions about the petroleum reservoir
63 potential of such sandstone bodies, the rock properties and diagenesis of the sandstones, and our understanding
64 of the potential consequences of the volcanic processes on oil/gas-field development (e.g. Kudu (offshore
65 Namibia), McLachlan 1990; Jerram et al. 1999a; Rosebank (UKCS), Helland-Hansen 2009; Schofield and
66 Jolley 2013; Anne-Marie (Faroes), Beswetherick et al. 2009; Benbecula (UKCS), Hitchen et al. 2013).
67 Currently knowledge is limited on the degree of igneous-related compartmentalization, to which igneous bodies

68 (intrusions or lava flows) contribute, and the role of volcanically induced diagenesis. It is also often unclear
69 whether lava flows are in hydraulic connection with interbedded siliciclastic units, which may increase the
70 overall reservoir volume of such units if they are, or make them less prospective if not. Clearly, an
71 understanding of the development of sediment-lava stratigraphy and how its diagenetic history is recorded is of
72 importance to understanding how these competing systems have interacted, with direct implications for
73 reservoir characterization.

74 In order to investigate sediment/lava stratigraphy further, we describe the diagenetic fingerprint of hydrothermal
75 activity on isolated sand bodies within a flood basalt pile, where contrasting diagenetic styles occur between
76 discrete sand bodies that are separated by tens to hundreds of meters by lavas and igneous dikes. We test the
77 hypothesis that the fluids responsible for differential diagenesis were spatially restricted by the igneous rocks,
78 thereby compartmentalizing the groundwater flow regime.

79 Our results show that vertical and subvertical igneous intrusions are responsible for compartmentalizing the
80 basalts and inter-basalt sediments (see also Rateau et al. 2013; Schofield et al. 2015; Senger et al., 2017) and the
81 lava flows allow fluid movement between isolated sand bodies. Lava flows contain potential fluid pathways in
82 vesicular, fractured, and brecciated regions, whereas the core regions of lava flows are more massive and
83 potentially form barriers to flow where not fractured (e.g, Watton et al. 2014). In addition to reporting on fluid-
84 flow compartmentalization using diagenetic fluids as a tracer, this contribution also describes how the diagenetic
85 effects of these fluids have acted as a reservoir-degrading mechanism within the affected sand bodies (both
86 porosity and permeability reduction). Further, the proposed mineral reaction is a natural example of the carbon
87 dioxide sequestration mechanism of Hangx and Spiers (2009), such that a natural analogue to proposed CO₂
88 sequestration mechanisms has been identified in a mixed basalt-siliciclastic system (e.g, Jones et al., 2016). This
89 has implications for the successful exploitation of similar systems for the long-term disposal of anthropogenic
90 CO₂ (e.g, Matter et al. 2016). The discussion is directed to the early stages of diagenesis in sediment/lava
91 interbedded sequences and contacts in the Paraná-Etendeka flood-basalt sequence, and its implications for
92 understanding fluid flow and petroleum prospectivity in similar settings (e.g, inter-basalt and sub-basalt
93 sediments in the Faroe-Shetland Basin, Rockall Trough, and inter-basalt sediments offshore Southern Atlantic,
94 e.g, Brazil, Angola, and Namibia, as well as early volcanic sequences in flood basalts and volcanic margins
95 globally).

96 **CASE-STUDY OUTLINE AND GEOLOGICAL SETTING**

97 The case study presented uses the Lower Cretaceous stratigraphy in NW Namibia (The Twyfelfontein and
98 Awahab Formations, about 134 Ma) (Mountney et al. 1998; Mountney et al. 1999a, 199b; Jerram et al. 1999a,
99 1999b; Jerram et al. 2000a, 2000b; Jerram and Stolhofen 2002; Dodd et al., 2015). These units represent an
100 exceptionally preserved example of where sediments have been buried and completely preserved within lava
101 sequences (e.g. Mountney et al. 1999a; Jerram et al. 2000a), with the lower parts of the Awahab formation
102 containing sandstone bodies which are isolated within the lava field (Jerram et al. 2000a). The rocks
103 (sandstones, volcanoclastics, basaltic lava flows) are cut by later dolerite dikes. The case study presented is in an
104 area named “Dune Valley” and is located in the foothills SW of Awahab (Mikberg) mountain, Huab Outliers,
105 Kunene Region, NW Namibia (Fig. 1). Desert exposure (70 % to nearly 100% outcrop) and nearly complete
106 preservation of lava-drowned barchanoid eolian dunes (Jerram et al. 2000a), now exhumed by preferential
107 erosion of basaltic lava, allow detailed sampling and mapping. Early diagenetic effects have been preserved due
108 to prolonged aridity (desert conditions have prevailed since the Cretaceous; e.g. Goudie and Eckardt 1999). The
109 arid Namibian setting contrasts with the South American correlative equivalent, the Botucatu and Serra Geral
110 Formations, where secondary diagenetic effects (large meteoric-water flux) in some cases have overprinted such
111 early features (e.g. França et al. 2003). Lack of exposure in South America makes detailed studies limited often
112 to quarries and coastal exposures (e.g. Petry et al. 2007, Waichel et al. 2008).

113 *Regional Geological Setting*

114 The term Huab Basin describes the basinal feature centered on the Huab River, containing sedimentary rocks of
115 the Palaeozoic–Mesozoic Karoo Supergroup and Mesozoic Etendeka Group (e.g. Horsthemke et al. 1990;
116 Jerram et al. 1999a; Mountney et al. 1999b), which rest on deformed Damaran basement rocks (500– 600 Ma)
117 (Fig. 2). The basin records the extensional tectonic regime and associated continental sediment deposition
118 relating to the breakup of Gondwana (Clemson et al. 1997; Jerram et al. 1999a), initially with deposition during
119 the Permian–Jurassic Karoo, followed by an erosional hiatus and subsequent Late Mesozoic rifting in the latest
120 Jurassic and Lower Cretaceous. The Huab Basin sedimentary rocks thin toward the south and lap onto the
121 Damaran basement, and clearly fill in a structurally bounded depression that roughly follows the present Huab
122 River (Mountney et al. 1999b). The study area (Figs. 1, 3) is situated within the Huab Outliers (Jerram et al.
123 1999a) south of the Huab River. The Huab Outliers preserve a complete section through the Huab Basin
124 sedimentary and volcanic sequence (Twyfelfontein and Awahab Formations).

125 The stratigraphic section of interest in this study is the transition from continental sedimentary rocks to
126 continental flood-basalt lava and crosscutting igneous intrusions (Fig. 2). This is marked by two formations: the
127 Twyfelfontain Formation and the Awahab Formation). The Twyfelfontain Formation was formerly known as
128 the Etjo/Cretaceous Etjo Formation (e.g. Horsthemke et al. 1990; Milner et al. 1995; Moutney et al. 1998;
129 Moutney et al. 1999a, 1999b; Jerram et al. 1999a, 1999b; Jerram et al. 2000a, 2000b). The current
130 Twyfelfontain Formation name was introduced by Stanistreet and Stollhofen (1999) and Schreiber (2006). In
131 this study, we use the term Twyfelfontain Formation as this clearly separates these Cretaceous rocks from the
132 Jurassic Etjo Formation rocks farther south in Namibia, and it is the current formation name used by the
133 Geological Survey of Namibia (cf. Schreiber 2006).

134 The Twyfelfontain Formation consists of predominantly eolian sedimentary rocks, occasional fluvial beds, and a
135 notable fluvial sandstone and conglomerate sequence at the base (known locally as “The Krone Member”,
136 Moutney et al. 1998). The Awahab Formation is composed of interbedded sedimentary rocks (again
137 predominantly eolian) and lavas at the base, and thick lava sequences higher up (Milner et al. 1995; Jerram et al.
138 1999a) (Fig. 2). The lava stratigraphy has been subdivided based on geochemistry of the constituent lavas (e.g.,
139 Milner et al. 1995; Jerram et al. 1999a). The lava stratigraphy is made up of olivine-rich lavas (low viscosity) at
140 the base, termed the Tafelkop lavas based on their geochemical type (Milner et al. 1995; Jerram et al. 1999a).
141 These then transition into basalts and basaltic andesites, termed the Tafelberg on geochemical type (Milner et al.
142 1995; Jerram et al. 1999a), and finally into silica-rich units (quartz latite) towards the top. In “Dune Valley” the
143 Tafelkop basalts are fed locally from dikes and the volcanic center called “Doros Crater”, to the south. At the
144 time of eruption they built up a sizable shield volcano centered on Doros (Jerram et al, 1999a; Jerram and Robbe
145 2001; Marsh et al. 2001). The more voluminous Tafelberg type lavas overlapped and buried this shield volcano,
146 and mark the end of the preserved sediments in “Dune Valley” (Jerram et al. 1999a; Jerram and Robbe 2001).
147 These more voluminous lavas, covered the existing topography and peneplained the area prior to the almost
148 complete blanketing of the region with large-volume silicic eruptions (known locally as quartz latites; Milner et
149 al. 1995). The silicic units mark the upper parts of the stratigraphy in this area and extend into the Paraná Basin
150 (Bryan et al. 2010). Within Dune Valley, the Twyfelfontain Sandstone is predominantly buried by Tafelkop-
151 type lava, which, in this location, is morphologically a compound-type lava (cf. Walker 1971; Jerram 2002),
152 with minor sediment in contact with Tafelberg-type basalts (massive inflated sheet and tabular flows) towards
153 the top of the sequence. Throughout the sequence, sills, dikes, and shallow intrusions are found associated with
154 the emplacement of the Paraná-Etendeka province in the Lower Cretaceous.

155

Lava-Sediment Interaction

156 At the onset of effusive volcanic activity, marking the start of the Parana-Etendeka igneous province, the
157 Twyfelfontein erg system (in Dune Valley) was sequentially buried with pahoehoe lava of Tafelkop type. The
158 lava flows passively drowned the dunes as they inflated and filled in the topography (Jerram et al. 2000a). This
159 resulted in the preservation of eolian features with very little disturbance (e.g. dune forms and topset beds)
160 (Jerram et al. 1999b, Jerram et al. 2000a), the process is summarized in Figure 4 (modified from Jerram et al.
161 1999b). Initially the desert contained large draa dune forms over 100 m high in places (Mountney et al. 1999a),
162 as part of the large desert sand sea (erg) system prevailing across the Paraná-Etendeka basins at the time (Jerram
163 et al. 2000a; Scherer and Goldberg 2007). Sand mobility, and volumes of available sand, were restricted by
164 successive burial by lava flows, such that second- and- third generation dunes resting on lava surfaces were
165 sediment starved, were reduced in overall thickness, and became barchanoid in shape in the upper parts of the
166 system (e.g. Mountney et al. 1998; Jerram et al. 2000a). Adjacent dunes were separated by distances of c. 100 m
167 during lava inundation (Figs. 3, 5, 6). When drowned by volcanic activity the barchans were hence completely
168 encapsulated by lava.

169

METHODS

170 The distribution of sand bodies within the lava sequences in Dune Valley was mapped out along with the main
171 types of diagenetic coloration, as seen in the field (Figs. 3 and 5). Once the outcrops were characterized,
172 samples were taken for further detailed analysis. A total of 23, 30- μm -thick, blue-resin-impregnated thin
173 sections, which were stained for potassium feldspar (HF etched and sodium cobaltinitrite treated) and carbonate
174 (alizarin red and potassium ferricyanide) were prepared and modal abundances of minerals measured using
175 standard point-counting techniques (500 points, see Grove and Jerram 2011 for uncertainty analysis), and
176 studied under both plane-polarized and cross polarized light. Chips from the 23 samples were also inspected
177 using a Hitachi TM1000 scanning electron microscope (SEM). Five samples were lightly crushed and analyzed
178 as an oriented powder on glass slides using a Bruker D7 X-Ray diffractometer using Cu K-alpha 1 radiation
179 (1.5406 Å). Calcite cements were identified in thin section using cathode luminescence and staining techniques
180 (e.g. alizarin red and potassium ferricyanide). Measurements of $\delta^{13}\text{C}$ and $\delta^{18}\text{O}$ values were made at Durham
181 University on four samples of calcite and corrected to international reference standards (including NBS 19 and
182 NBS 18 calcite). Stable-isotope data for calcite are presented relative to VPDB. Five samples were analyzed for
183 major elements using a Panalytical PW2404 wavelength-dispersive sequential X-ray spectrometer at the

184 University of Edinburgh. Permeability measurements were taken on 20 samples using a probe permeameter at
 185 the University of Aberdeen (e.g, Hurst and Goggin 1995), held in a clamp. Multiple measurements were carried
 186 out on each sample (up to 19) unless permeability recorded 0 md after several attempts. Permeability was also
 187 measured on four 26 mm core plugs (also measured with the probe permeameter) using a Frank Jones Hasler
 188 sleeve-type porosimeter with a confining pressure of 400 psi (2.8 MPa) at the University of Aberdeen. Porosity
 189 was calculated as total optical porosity from thin-section analysis (by point counting). As a control, sample
 190 NG52 was collected from the major erg (equivalent normal red sand, Type 1) tens of meters away from any
 191 igneous contacts and does not display any diagenesis related to igneous activity.

192 **DIAGENESIS**

193 *Petrology and Mineralogy*

194 Three types of diagenesis are identified in the sandstones, and are petrographically and mineralogically
 195 described in detail below. They can be found in the isolated sand bodies in “Dune Valley” and also in the major
 196 and minor erg units (e.g, Jerram et al. 1999a), which are found stratigraphically below the lava-interbedded
 197 isolated dunes. “Type 1” diagenesis is found in red isolated dunes, and red areas of the main and minor erg
 198 system. “Type 2” diagenesis is found in white isolated dunes, and in patches within the main and minor erg
 199 system. Both red and white isolated dunes display “Type 3” diagenesis near to hot lava contacts, with no
 200 appreciable difference between red or white isolated dune contact zones, as well as on the hot-lava/sediment
 201 contacts in the major and minor erg units (e.g, Jerram and Stollhofen 2002). The three types of diagenesis and
 202 how they are manifest in the sandstones are described in detail in the following sections, concentrating first on
 203 the key observations for each, then a short discussion about the diagenesis types, before a broader discussion on
 204 the implications for understanding the main controls on diagenesis and fluid flow.

205 *Type 1 Diagenesis Observations- Burial Diagenesis*

206 Type 1 diagenesis represents the normal burial-related diagenesis, without the influence of the igneous system.
 207 This burial diagenesis is exhibited in the isolated red dunes, where the original mineralogy has not been
 208 overprinted by igneous-related affects. Isolated red dunes are compacted subarkosic litharenites. They are
 209 composed of rounded eolian grains in well sorted grain-flow lamellae (fine to coarse sand) and less well sorted,
 210 rounded to subrounded grain fall (very fine to fine sand) lamellae (e.g, Howell and Mountney 2001). The
 211 detrital grains comprise quartz, potassium feldspar, plagioclase, lithic grains, and opaque minerals (ilmenite)

212 (Table. 1). Ilmenite is not widely disseminated and appears to form small placer deposits controlled by grain
213 density. Detrital grains are coated with hematite, which gives the red coloration (Figs. 7C, 8A). Here sutured
214 quartz grains suggest compaction through quartz dissolution; this appears to have been one of the main
215 diagenetic processes (e.g, Fig. 7C sutured grains). Cements are rare, although occasional quartz overgrowths are
216 present on some grains (~ 1.5%). Crushed potassium feldspar grains exhibiting shear and dilation along
217 cleavage planes were also observed consistent with the work of Dickinson and Milliken (1995), who initially
218 described the formation diagenesis. Porosity averages 15.2% in Type 1 sandstone and permeability averages
219 1095 md.

220 In the present study “Dune B” (Figs. 3, 5, 6) has been chosen as the type example of Type 1 diagenesis because
221 of its superior vertical exposure (2.5 m) allowing excellent access. It should be noted that “Dune B” can be
222 found only 120 m south of “Dune A” (a white dune) (Fig. 5), and in close proximity to many other isolated
223 dunes which are white. In the field, Type 1 dunes are clearly identified compared to Type 2 dunes based on this
224 red or white color (e.g, Fig. 5). Red sand is also dominant in the minor and major erg units, stratigraphically
225 below (Fig. 2), separated by lava (e.g, Jerram et al. 1999b).

226 *Type 2 Diagenesis Observations- Isolated White Dunes*

227 White (yellow or white in weathered outcrop) sandstones are distributed throughout the Twyfelfontein
228 Formation, and where they occur as isolated dunes due to flooding by lavas (Fig. 4), there appears to be no
229 intrinsic pattern to their distribution, occurring with red isolated dunes in close proximity (Fig. 5A, C). At
230 outcrop scale, the only difference appears to be color, with sedimentary structure showing no difference in
231 morphology (e.g, Fig. 5B, C). It can be shown that the white dunes were deposited in the same way as the red
232 dunes as isolated migrating barchanoid dunes which were preserved by burial under lava flows (e.g, Mountney
233 et al. 1998; Jerram et al. 2000b). The question then arises regarding the diagenetic history of these white
234 sandstones, and how it differs from the red eolian units.

235 Thin sections of the white sandstone indicate that it is also a subarkosic litharenite. Rounded to subrounded
236 quartz grains occur in grain-fall and grain-flow lamellae, which are usually well sorted. Detrital grains are
237 similar to those in the red dunes. However, feldspar grains are visibly corroded or are completely replaced by
238 clay. Plagioclase feldspar grains show the most intense alteration, with no petrographically identifiable grains
239 being encountered under optical microscopy that could be identified based on albite twinning. Any plagioclase
240 encountered was identified based on lack of yellow staining from sodium cobaltinitrite and by ruling out

241 identification as quartz (crossed-polars examination); therefore plagioclase has probably been petrographically
242 overestimated (Table 1; Appendix 1); most counted plagioclase grains are probably in fact completely
243 kaolinitized pseudomorphs (SEM analysis confirms this). Potassium feldspars in white sandstone samples are
244 also frequently corroded or partially transformed into clay minerals (Fig. 8B). Hematite grain coatings are
245 absent in the white sandstone, but opaque detrital minerals are still present, as are occasional aggregates of
246 hematite in pore spaces (this may be a later oxidation product of pyrite). The assemblage of authigenic minerals
247 is different from that of the red dunes and can be classified using petrographic techniques. Under the
248 petrographic microscope the assemblage is composed of kaolinite, calcite, and occasional quartz overgrowths.
249 Calcite and kaolinite are usually associated, and both replace feldspars and fill pore space. Porosity in Type 2
250 sandstone is lower than the Type 1 sandstone, averaging 4.8%. Permeability values in the white sandstone
251 increase from negligible values in the Type 3 (see below) contact zone, but do not exceed 44 md (Figs. 9, 10),
252 with an average of 26 md.

253 SEM examination of the samples confirmed the identified assemblage from light microscopy and enabled the
254 additional identification of pore-lining böhmite (as pisolitic aggregates (Fig. 11), cf. Wu et al. 2012; Cai et al.
255 2009). Böhmite proved to be a common lining of pores in the white sandstone under the SEM, with all white
256 samples having the mineral in abundance. It is not clear if there are any specific trends of böhmite throughout
257 the dunes due to its difficulty to detect and quantify with optical microscopy. Kaolinite can be seen in SEM to
258 form books that fill pore space and aggregates that replace feldspars (e.g. Fig. 11D). Calcite in SEM is always
259 found to be associated with kaolinite and frequently fills pores (Fig. 11A).

260 X-ray diffraction analysis was performed on sample NG29, which comes from 3 m below the hot contact in
261 isolated white Dune A (Fig. 12). This distance is significantly outside the ~ 30 cm contact zone where Type 3
262 diagenesis occurs. The spectrum for NG 29 was compared with NG32 isolated red Dune B, 2 m below the
263 contact (limited by outcrop exposure). The white sandstone did not display any plagioclase peaks (e.g. anorthite
264 100 peak, 3.19 Å (27.96° 2θ)) and orthoclase peaks were weakened. Kaolinite (7.17 Å (12.35 ° 2θ) and 3.58 Å
265 (24.83 ° 2θ) peaks are present in the white sand (not found in the red sand). Böhmite was not detected in XRD,
266 despite it being an obvious phase in SEM. This is probably due to its low volume abundance. Calcite did not
267 show a clear spike, despite being seen in optical microscopy and SEM.

268 Given that all of the isolated dunes were deposited at the same stratigraphic level and subsequently either
269 bleached white or not, it is instructive to determine how the two main types of diagenesis in the dunes evolved

270 and whether there has been any net flux of elements in or out of each system. X-ray fluorescence analyses were
271 performed on five samples with the aim of testing enrichment or depletion in elements as a result of dune
272 bleaching- specifically, to test the hypothesis that there was depletion in relative iron abundance in white dune
273 sandstones. For analysis, the data were normalized to NG52, which is considered to be background red
274 sandstone. The geochemical differences between red and white dunes (Fig. 13A) support the petrographic
275 observations. Iron and sodium are depleted in white dunes compared with NG52 and NG32. Calcium is enriched
276 in the white sample, and LOI is ~ 7 times that of NG52. Aluminum is approximately equal in Type 1 and Type 2
277 sandstones.

278 *Type 3 Diagenesis Observations- Hot Lava Contacts*

279 The upper surfaces of fossil dunes in the study area often display features such as topset beds and eolian ripples,
280 as well as preserved lava-emplacment features such as striations and lava imprints (see Jerram et al. 1999a;
281 Jerram et al. 2000a; Jerram and Stollhofen 2002 for description). These features indicate that the upper dune
282 surface was contemporaneous with and covered by flowing lava. Type 3 diagenesis is found only in these upper
283 dune surfaces. Basal surfaces (i.e, cold contacts: sands that were deposited on top of the solid cooled upper
284 surface of lava) usually display Type 1 or Type 2 depending on overall dune diagenetic type. Generally, there is
285 no evidence of significant early weathering of the cooled-lava top surfaces, indicating that little time passed
286 between the emplacement of the lava and migration of sand dunes (Jerram and Stollhofen 2002).

287 For both Dune A (NG26) and Dune B (NG31) contacts, porosity is always found to decrease towards the
288 formerly hot contact (Fig. 9 A). Reductions in porosity in the sandstones start to become apparent at depths of <
289 2 m from the contact with the base of lavas. At these depths porosity values are 15–20%, and they decrease to <
290 1% at the contacts with the lava. Permeability in red dunes increases rapidly away from the contact, reaching
291 background permeability of between 100 md and 1000 md at depths of ~ 30 cm below the once-hot lava contact.
292 At hot-lava contact zones, permeability approaches negligible values (Fig. 10 A). Permeability in white dunes
293 does not return to these normal background values outside of the contact zone, due to Type 2 diagenesis.

294 The modal proportion of authigenic calcite and authigenic clay (chlorite identified, other clays undifferentiated)
295 increase toward hot contacts (Figs. 7, and 14). In red sandstones, clay increase is apparent only at the contact.
296 Porosity loss in the sediments occurred through both compaction and mineral authigenesis, as is shown by the
297 porosity loss measurements (COPL % and CEPL %) (see Appendix. 1). In both dune types the proportions of
298 opaque minerals (mainly hematite and goethite rims on detrital grains) increase slightly toward hot contacts;

299 importantly, both red and white dunes have high abundance of opaque mineral near the hot lava contact. Calcite
 300 increases towards lava contacts in red dunes but does not in white dunes. Compactional porosity loss, calculated
 301 using the method from Lundegard (1992), increases towards contacts (between ~ 30 cm and the contact (Fig.
 302 9B)). Cementational porosity loss (Lundegard 1992) shows more variation but is highest near contacts. Detrital
 303 mineralogy shows little variation with proximity to hot contacts (red dunes).

304 The results of the X-ray diffraction are summarized in Table. 2; the data generally confirm the petrographic
 305 observations (Fig. 7). Both red and white dune contacts produce strong calcite peaks at 3.035 Å (~ 29.46° 2θ).
 306 NG 31 produced a peak at 3.15 Å (28.3 ° 2θ) that corresponds to fluorite; this supports a tentative petrographic
 307 identification of this mineral. Fluorite pore fills are also occasionally found in the Twyfelfontein Formation
 308 elsewhere under other hot contacts. NG26 produced clay peaks at 7.17 Å (12.35 ° 2θ) and 3.58 Å (24.83 ° 2θ);
 309 the strength of the 3.58 Å peak supports the interpretation of clinochlore as the clay phase, but kaolinite is also
 310 possible. Hematite was not detected with XRD, possibly due to its presence in very low abundances
 311 (petrographic observations overestimating its abundance).

312 In samples from hot contacts (Type 3) (Fig. 13 B) both samples (red and white dunes) are geochemically similar
 313 with the exception of manganese, which may relate to the presence of Ilmenite. Both contacts are enriched in
 314 magnesium and calcium, and show minor enrichment in iron. LOI is also higher than NG52, which is an
 315 indication of the presence of the release of trapped volatiles (H₂O and CO₂) during ignition, probably from
 316 within the clay minerals and carbonate. Note that the enrichment in calcium is ~ 27 times that of NG52. Basaltic
 317 rocks can contain up to 25% by weight of calcium, magnesium, and iron (Matter et al. 2016).

318 *Stable-Isotope Analysis of Calcite Cements (Type 2 and Type 3 Diagenesis)*

319 Only samples containing calcite could be analysed; therefore there are stable-isotope data only for Type 2 and
 320 Type 3 sandstone, Type 1 not having any calcite. Three samples from Type 2 (white) and one sample from Type
 321 3 returned an adequate CO₂ yield for stable-isotope analysis. When δ¹³C is plotted against δ¹⁸O, the Type 2
 322 (white) sandstone calcite forms a field separate from Type 3 diagenesis calcite (Fig. 15A). δ¹⁸O and δ¹³C are
 323 heavier for Type 2 calcite (δ¹⁸O mean = -2.9‰ V-PDB, δ¹³C mean = -0.6‰ V-PDB) than for Type 3 calcite
 324 (δ¹⁸O mean = -13.6‰ V-PDB, δ¹³C mean = -9.3‰ V-PDB).

325 In order to understand the origin of the Type 2 and Type 3 calcite, modelling was performed to test what water
 326 temperature and water compositions could produce the observed calcite compositions. The models were set up

327 using a range of water compositions: Cretaceous meteoric water in Namibia ($\delta^{18}\text{O} \approx -4.7$ to -5.1% SMOW) (see
328 below for estimation method) and magmatic water ($\delta^{18}\text{O}$ 7‰ SMOW to 13‰ SMOW, Brownlow, 1996).
329 Fractionation constants $A = -3.39$ and $B = 2.78$ (O'Neil et al. 1969) were used. The composition of meteoric
330 water in Lower Cretaceous during the Etendeka volcanism was estimated by taking the Lower Cretaceous
331 Namibia palaeolatitude of 29° to 32° south from Scotese (2001) and the variation of $\delta^{18}\text{O}$ with latitude from
332 Bowen and Wilkinson (2002).

333 The model for Type 2 calcite (Fig. 15B) shows the Lower Cretaceous meteoric water would precipitate calcite
334 with the observed values at temperatures between 20°C and $< 0^\circ\text{C}$. When magmatic values for water are
335 modelled, temperatures required are between 50°C and 150°C .

336 The model for Type 3 calcite (NG31) (Fig. 15B) shows that precipitation from Lower Cretaceous meteoric
337 water would have been at temperatures between 50°C and 60°C . Magmatic waters would have precipitated
338 calcite at temperatures between 180°C and 330°C .

339 The modelled temperatures for Type 3 calcite are consistently hotter than Type 2 calcite, consistent with the
340 hypothesis that the Type 3 calcites were eogenetic, formed during lava cooling at the hot lava-substrate contact.
341 The Type 2 calcites show low temperatures that are not consistent with precipitation from a meteoric aquifer
342 given the observed mineral assemblage association and the likely aquifer temperature in a hot, arid setting. For
343 instance, the present-day aquifer temperature around the study area in Namibia is $> 25^\circ\text{C}$ at even shallow
344 depths (20-50 m) (Marx, 2009). More realistic temperatures are possible when the water is enriched with O^{18}
345 over that of the predicted meteoric water. A possible-magmatic water component of the aquifer is therefore
346 supported, and the aquifer could have comprised meteoric water, enriched by a magmatic-water component
347 sourced from degassing igneous intrusions. The Type 3 calcite precipitated before the Type 2 calcite (both red
348 and white dunes have Type 3), and therefore if precipitated in the subsurface should show cooler temperatures
349 reflecting shallower burial (assuming normal burial). However, the temperatures modelled are hotter. This
350 suggests that meteoric water is unlikely because if both were precipitated in the subsurface within a meteoric
351 water derived aquifer during normal burial, the earlier cement would show lower temperatures, which is
352 opposite to the observation. The temperatures modelled from magmatic waters are achievable at the contact with
353 a basalt lava flow (c. 1200°C). Therefore, a magmatic origin of the Type 3 calcite is suggested.

354 The $\delta^{18}\text{O}$ and $\delta^{13}\text{C}$ values for the calcites for Type 2 and Type 3 calcites are compared with other calcites in
355 Figure 15A. Neither calcite in this study directly overlies any of the fields chosen from the literature. The Type

356 3 calcite plots closer to the high-temperature geothermal calcites than Type 2, reflecting its higher-temperature
357 origin from possible magmatic volatiles. The Type 3 calcite is isotopically light, similar to what would be
358 expected for either a magmatic carbon or a biologically derived carbon. Figure 15A (fields 10 and 11) shows
359 that calcretes formed under biological influence plot distinctly from the Type 3 calcite, supporting a magmatic
360 rather than a biological origin. Further, no evidence of vegetation (e.g, fossil roots) has been found in the
361 Twyfelfontein Formation. The Type 2 calcite plots closest to the geodes in the Paranã Basalts from Brazil (Gilg
362 et al. 2003) and calcites found in sedimentary beds associated with Jurassic basalts in Namibia (Gierlowski-
363 Kordesch et al, 2015), supporting the igneous association. Both the red and the bleached sandstones of the
364 Navajo and Entrada Sandstone Formations (Chan et al, 2000; Garden et al, 2001; Beitler et al, 2005) are plotted
365 in Figure 15A, none of which overlie the Type 2 white sandstone calcite in the Twyfelfontein Formation,
366 supporting the hypothesis that the origin of the bleaching is different from the hydrocarbon-migration-related
367 process observed in the Navajo and Entrada Formations.

368 In summary, the stable-isotope data suggest that the Type 3 calcite formed under hot conditions, with oxygen
369 and carbon of a likely magmatic origin and that the Type 3 calcite formed in an aquifer with meteoric and
370 magmatic components under cooler conditions, likely between ~ 25° C and 150° C.

371 *Type 1 Diagenesis- Discussion of Burial Diagenesis*

372 Dickinson and Milliken (1995), who first described the sandstone diagenesis in the Huab area, concentrated on
373 the sandstones beneath the lava flows and made no distinction between the different red or white diagenesis
374 types or indurated sediment found at the hot lava contacts. They readily observed features associated with burial
375 diagenesis and deformation of grains, but they concluded that the conditions under which brittle deformation
376 occurred in the sandstone were poorly constrained because the burial history is uncertain. Dickinson and
377 Milliken (1995) principally investigated the role of brittle deformation and pressure solution away from the
378 igneous affected sandstones and therefore did not describe the white sandstone or the lava-sediment contacts;
379 their study can be taken as a good description of the Type 1 diagenesis.

380 It is clear that there has been significant erosion of the original lava sequence to expose the stratigraphy in the
381 Huab Basin, although the exact extent and thickness of the original volcanic stratigraphy in flood basalts is
382 notoriously difficult to estimate (e.g, Jerram and Widdowson, 2005). The overall thickness of the Paranã -
383 Etendeka lavas, and thus the potential depth of subsequent burial, has been estimated to be as thick as 3-4 km
384 based on the overall Paranã -Etendeka stratigraphy (e.g, Peate 1997) and from apatite fission-track analysis (e.g,

385 Raab et al. 2005). Although such estimates contain a significant error, it is likely that the sandstones considered
386 in the present study have suffered some burial diagenesis under a significant overburden of volcanic
387 stratigraphy. We propose that Type 1 diagenesis seen in the red sandstones is a function solely of this burial
388 diagenesis and represents sandstone that has not been subjected to any hot-contact diagenesis (Type 3) or to a
389 flux of fluid that was responsible for Type 2 diagenesis.

390 *Type 2 Diagenesis- Discussion of Isolated White Dunes*

391 Porosity reduction due to compaction processes visually appears more intense in thin sections of the white
392 sandstone than in the red sandstone (e.g. thin-section photomicrographs in Fig. 8A. vs. in Fig. 8B; porosity
393 values in Fig. 9). Increased visual compaction may have resulted from the weakening of feldspar grains during
394 dissolution. These grains were then deformed to fill adjacent pores, or dissolved, thus reducing matrix strength.
395 When quantified however, COPL is not significantly different in red or white dunes (Fig. 9). Figure 9 shows
396 that it is cementation (CEPL) that contributes most to the additional porosity loss. Figure 10B shows a clear
397 separation between the Type 1 and Type 2 diagenesis in the permeability-porosity cross plot, with little overlap,
398 despite relative position in the isolated dunes being approximately equal.

399 Modal analysis of thin sections indicates that the white dunes have up to four times the amount of clay and five
400 times the amount of calcite as the red dunes (Fig. 14D). Authigenic calcite shows no correlation with distance
401 below lava in the white dunes. The white dunes contain both calcite generated during the emplacement at hot
402 contacts and calcite formed during bleaching. Conversely, there is a negative correlation in red dunes between
403 calcite and distance below the lava, as calcite here is controlled solely by Type 3 diagenesis in the absence of
404 Type 2 diagenesis.

405 Authigenic quartz occurs in slightly lower abundance in white dunes and shows significant variability and no
406 correlation with distance below the lava. The lower abundance of authigenic quartz may be due to pore-lining
407 clay minerals inhibiting quartz precipitation during further burial, compared to the clay-absent red sandstone.
408 Opaque minerals are less abundant in the white sandstone (the hematite grain coating being absent) and show a
409 weak negative correlation with distance below lava, due to the Type 3 diagenesis at the contact (locked-in
410 hematite); in the red sandstone, opaque minerals show no correlation with distance (Fig. 14C). The difference
411 between the abundances of authigenic minerals has been tested using the statistical “Students T-Test” (e.g.,
412 Hazewinkel 2001). The results from this show that porosity, permeability, and abundances of authigenic quartz,
413 authigenic calcite, and authigenic clay are statistically (at the 95% level or greater) different between red and

414 white dunes (Table. 3). Abundance of opaque minerals was not found to be statistically different. This is
415 because the hematite was probably being redistributed from grain coatings to the identified pore-filling
416 aggregates, noted also as iron oxide nodules in outcrop. The likely process is reduction of hematite grain
417 coatings and reprecipitation as pyrite nodules, which are oxidized during exhumation into hematite.

418 The interpretation of the geochemistry suggests that a flux of fluid must have been necessary to allow
419 enrichment and depletions in elements. If feldspars were simply transformed into the authigenic minerals, with
420 no loss or gain from the system, the bulk rock would be similar to NG52. Importantly, the loss of sodium in the
421 white dune shows that only the calcium from dissolving plagioclase was being completely sequestered into
422 authigenic minerals (otherwise sodium would mirror calcium). No sodium-containing authigenic minerals were
423 found in quantity, sodium being mobile in groundwater (White 1957). The sodium was probably transported out
424 of the system in solution; it should be noted that sodium is commonly found at elevated concentrations in
425 thermal springs of volcanic origin (White 1957). Aluminum is conserved, presumably being rapidly
426 incorporated into böhmite and kaolinite. The calcium enrichment suggests that calcium was being transported
427 from elsewhere in the system and being precipitated in white Dune A. A possible source for this calcium is other
428 sand bodies being depleted or volcanic glass and/or plagioclase in lavas part of the volcanic pile. Interaction
429 with the lavas in the pile is also consistent with the possibility of basalt-water interaction enriching the
430 hydrothermal water in heavy oxygen and is supported by the observation that the Tafelkop basalts are vesicular,
431 hence probably permeable. High LOI confirms that NG29 is rich in hydrated minerals (clays) compared to
432 NG52. Note that the depletion of iron in the white sandstone is minor, possibly as a function of the low original
433 iron concentration, but more likely supporting the hypothesis that iron was being locally redistributed into
434 nodules, with only a minor amount leaving the system.

435 These observations together depict a system in the isolated white dunes where hematite was being dissolved
436 from grain rims, and böhmite, kaolinite, and calcite were being formed at the expense of feldspar. These mineral
437 transformations resulted in bleached and compacted sandstone, with reduced primary porosity.

438 *Type 3 Diagenesis- Discussion of Hot Lava Contacts*

439 The observations of Type 3 diagenesis support the interpretation that contact diagenesis was an early-stage
440 phenomenon, during emplacement and cooling of the lava. This is also supported by Type 1 and Type 2
441 diagenesis not affecting upper-contact-zone sediments in dunes that have been affected by Type 3 diagenesis.
442 This variation in diagenesis was initially described as “hot contact” diagenesis (Jerram and Stollhofen 2002). It

443 is proposed that when the lava was emplaced onto the eolian sand substrate, volatiles would have been
444 degassing (likely components include water, carbon dioxide, chlorine, fluorine, sulfur dioxide, hydrogen sulfide
445 and carbon monoxide as major components (e.g. Delmelle and Stix 2000; Lowenstern 2001; Simmons and
446 Christenson 1994; Shevenell and Goff 1993; White 1957), flowing following a pressure gradient towards
447 atmospheric pressure. H₂O is the most common volcanic gas, followed by CO₂, although in gases liberated from
448 basaltic magmas CO₂ sometimes exceeds water (Lowenstern 2001). During ascent of the magma to eruption,
449 CO₂ begins to exsolve before H₂O because of lower solubility in magma and remains as a low-density vapor
450 phase (Lowenstern 2001) as vapor filled vesicles in the molten magma. As the magma ascends to shallow
451 depths (1–4 km) H₂O and CO₂ degassing is forced (Lowenstern 2001). Erupting magma should then contain
452 vesicles comprising vapor-phase volcanic gas, dominated by CO₂ and H₂O, with proportions dependent on rate
453 of ascent. Most of these volatiles are released into the atmosphere during eruption (e.g. a fire fountain). The
454 stable-isotope evidence from Type 3 diagenetic carbonates, however, suggests that lava flows must still contain
455 enough magmatic CO₂ (vapor phase vesicles) at the time of emplacement to form the observed cements. We
456 propose the following mechanism for the presence of magmatic CO₂ in the immediately sub-basalt sand: The
457 pore space in the unconsolidated sand would have been at atmospheric pressure, so when the newly emplaced
458 lava cooled, a proportion of the gases would have invaded the pore space (driven by pressure gradient) and
459 reacted with the sand. This occurred with feldspar first (supported petrographically by the apparent increase in
460 feldspar breakdown to clays). Feldspar decomposition would have reduced feldspar strength, facilitating
461 mechanical compaction by rearrangement of grains. Note that the increased compaction is not apparent farther
462 than ~ 30 cm below the contact. Remaining porosity was filled by calcite, with carbon being sourced from
463 degassed magmatic CO₂ and calcium being sourced from reacting volcanic glass and plagioclase (igneous and
464 detrital). Mild hydrothermal activity is therefore inferred to have existed around the contact (in modern settings
465 this would be manifested on the lava surface as steaming fumarole vents). These observations are consistent
466 with the “hot” contacts seen between the lowermost lavas and both the major and minor erg sediments (Jerram
467 et al. 1999b; Jerram and Stolhofen 2002). This suggests that, if indeed the contact effects described are eogenic
468 (early diagenesis) as proposed, a low-porosity and low-permeability cap to individual isolated dunes would have
469 been formed, before any significant burial (and therefore Type 1 or more importantly Type 2 diagenesis). There
470 is also evidence for former hydrothermal activity during lava emplacement in the form of a fossil fumarolic
471 pipe, which was found where lava bulldozed into the sand as an invasive flow, and subsequently degassed
472 through the loose sand above. The XRF analysis suggests elemental flux into the system (magnesium and

473 calcium). We infer that enriched magnesium and calcium are hosted in the calcite cement and iron and
 474 magnesium are in the chlorite. If the elements were simply redistributed from feldspars during the Type 3
 475 diagenesis, there should be no enrichment in these elements. It is therefore proposed that calcium, magnesium,
 476 and iron are at least partially sourced from the overlying lava, probably during cooling and hydrothermal
 477 decomposition of volcanic glass.

478 **UNDERSTANDING THE MAIN DIAGENETIC CONTROLS**

479 Most of the volume of the intra-lava sediments in this study are affected by either Type 1 (burial diagenesis, red
 480 sandstone) or Type 2 (white sandstone) diagenesis, with Type 3 diagenesis volumetrically minor, restricted to
 481 relatively thin contact zones. What is driving this variation? The petrographical, mineralogical, and geochemical
 482 differences between isolated red dunes (Type 1 diagenesis) and isolated white dunes (Type 2 diagenesis) have
 483 been established. Chemical bleaching of sandstones is not rare; it has been documented elsewhere, commonly as
 484 a result of hydrocarbon migration through sandstone (Moulton 1926; Surdam et al. 1993; Kirkland et al. 1995;
 485 Parry et al. 2004; Schöner and Gaupp 2005; Ma et al. 2007). Bleached zones have been used to indicate
 486 migration pathways of hydrocarbons and to infer the existence of emptied reservoirs (Kirkland et al. 1995;
 487 Beitler et al. 2003; Beitler et al. 2005).

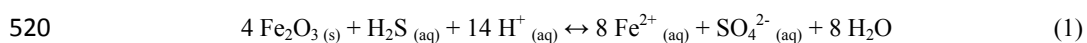
488 Where hydrocarbons have migrated through red sandstones, the bleaching has been attributed to acidic, reducing
 489 conditions (e.g. Ma et al. 2007; Surdam et al. 1993). These conditions can be achieved by biologically mediated
 490 oxidation of CH_4 to produce CO_2 and simultaneous reduction of SO_4^{2-} to H_2S (Kirkland et al. 1995). In such a
 491 reaction, the CO_2 and H_2S are achieved in conditions where dissolved H_2S (present as HS^-) reacts with ferric
 492 iron oxide (hematite) to form soluble ferrous iron. The HCO_3^- reacts with Ca^{2+} and Mg^{2+} to form carbonate
 493 minerals (Surdam et al. 1993; Kirkland et al. 1995). Dissolved ferrous iron and H_2S would not necessarily react
 494 immediately to precipitate as iron minerals (e.g. pyrite) and can migrate in pore waters (Kirkland et al. 1995).
 495 These conditions could also be achieved without contemporary biological mediation, as many hydrocarbons are
 496 associated with H_2S and CO_2 . A petrographic study of bleached sandstones has documented alteration of
 497 feldspars to clay (kaolinite) in these settings (Ma et al. 2007).

498 The migration of hydrocarbons is an unlikely mechanism for the bleaching (Type 2 diagenesis) of the
 499 sandstones in the study area because (A) there is no significant source rock in the thin underlying Karoo
 500 sequence this far south in the Huab Basin, and (B) hydrocarbon residues have not been observed in the field or
 501 during subsequent petrographic studies (including with UV light). However, the same chemical species required

502 (H₂S and CO₂) can be generated by magmatic degassing (e.g. Henley and Ellis 1983; Rye 2005; Delmelle and
 503 Stix 2000), probably during magma solidification (Arnórsson 1986) and are common in hydrothermal systems
 504 (e.g. White 1957; Henley and Ellis 1983). We infer that the fluids that passed through the isolated dunes of the
 505 Twyfelfontein Formation were hydrothermal in origin and were enriched in magmatic gases originating from
 506 degassing mafic intrusions at depth. It should be noted that many dolerite sills and dikes can be found in the area
 507 (e.g. Marsh et al. 1991; Duncan et al. 1989; maps presented in this study).

508 Our observations test this hypothesis. Firstly, both red and white isolated dunes were deposited at similar or the
 509 same stratigraphic levels, and have identical detrital compositions; this is illustrated by the fact that the Type 3
 510 diagenesis affects both the red and white dunes. The eogenic Type 3 diagenesis effectively “locked in” the
 511 reduced-porosity contact zone at an early stage, isolating the detrital red sediments from later large fluid fluxes.
 512 The oxidation and coating of the sand grains with hematite before deposition is supported by our observations of
 513 present-day migrating red dunes in the Namib desert and by numerous other examples cited (e.g. Folk 1976 and
 514 references therein).

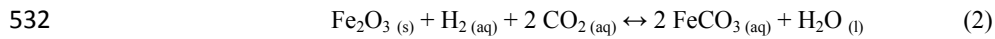
515 Secondly, considering that both the red and white isolated dunes were deposited as red-hematite-coated eolian
 516 sands, the white isolated dunes must result from chemical bleaching. It is proposed that this bleaching may have
 517 resulted from reaction of grain-coating hematite with H₂S in hydrothermal groundwater, which has circulated
 518 through white dunes only. Hematite is reduced to form soluble ferrous iron that is transported away in solution
 519 (Fe₂O₃ depletion, Fig. 13B):



521 $\text{hematite} + \text{hydrogen sulfide} + \text{hydrogen (acid)} \leftrightarrow \text{iron} + \text{sulfate} + \text{water}$

522 This reaction should produce pyrite as noted by Kirkland et al. (1995), which has not been directly identified in
 523 the isolated white dunes. Pyrite is however present in the basalt and occasional hematite nodules are present in
 524 the white sandstone. These hematite nodules may be the later oxidation product of diagenetic pyrite. If no pyrite
 525 was present in the white sandstone it could suggest either (A) that the Fe²⁺ and SO₄²⁻ were able to migrate into
 526 the basalt before to precipitating or (B) that any H₂S in the aquifer rapidly reacted with the iron-rich basalt
 527 before to reducing iron in the red dunes. If the latter is true, the above reaction (1) was doubtfully in operation in
 528 the white dunes. An alternative explanation that requires less acid and no sulfur is that of a hydrothermal system
 529 with abundant dissolved hydrogen. Hydrogen could have been sourced from hot hydrothermal water interacting

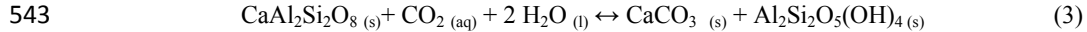
530 with basalt (Stevens and McKinley 2000) or from magma degassing at depth (Arnórsson 1986). Hydrogen and
 531 carbon dioxide could then bleach the sandstone:



533 hematite + hydrogen + carbon dioxide ↔ iron carbonate + water

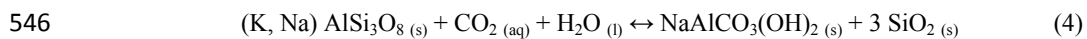
534 The ferrous-iron carbonate would have then been transported away in solution (e.g. King, 1998).

535 Thirdly, the feldspar dissolution and mineral authigenesis observed in the sandstones in the study area is inferred
 536 to result from CO₂-rich hydrothermal fluids. White dunes are almost completely devoid of plagioclase feldspar
 537 (XRD analysis) and show reduced-strength orthoclase XRD peaks compared to red sandstone. Authigenic
 538 kaolinite, böhmite, and calcite, found in the white sandstone (Type 2), are not found in the red sandstone (Type
 539 1) and are suggested to have formed at the expense of the feldspars during reaction with CO₂. Hangx and Spiers
 540 (2009) proposed and tested reactions between plagioclase feldspars and CO₂-H₂O under laboratory conditions
 541 simulating hydrothermal conditions. Both albite and anorthite were reacted under a variety of pressure and
 542 temperature conditions (200– 300 °C and 6– 18 MPa) with the aim to test the ideal reactions:



544 anorthite + carbon dioxide + water ↔ calcite + kaolinite

545 and



547 albite + carbon dioxide + water ↔ dawsonite + silica

548 Hangx and Spiers' (2009) results failed to fully replicate the above reactions and instead produced clays
 549 (kaolinite and smectite or illite), böhmite and a nickel, iron-hydrocalcite phase derived from their reaction
 550 vessel. Dawsonite and calcite were not produced in Hangx and Spiers' (2009) experiments, possibly due to
 551 subcritical solution state for crystal nucleation and conditions not being alkaline enough for dawsonite
 552 precipitation. Given sufficient time for further dissolution of plagioclase, carbonate phases would be anticipated
 553 (Hangx and Spiers 2009). It is proposed that in the white sandstone the Type 2 diagenesis is a natural analogue
 554 for the reactions observed by Hangx and Spiers (2009) based on the identical mineral reaction being observed.
 555 Calcite in the natural Type 2 white dunes is inferred to be the result of trace amounts of pre-existing carbonate

556 dust (common in eolian environments – Maurice Tucker, personal communication), and easily sourced locally
557 by the erosion of carbonate-rich Precambrian basement rocks in the region. This dust provides the nuclei for
558 calcite precipitation noted to be absent in Hanx and Spiers' (2009) experiments, as well as additional calcium
559 and carbonate. The basalt-plagioclase-CO₂ reaction between the lava flows and sediments in our natural
560 geological system produced enough Ca²⁺ ions for the additional calcite cementation to take place. This supports
561 the proposed origin of the diagenetic fluids and suggests timing coincident with emplacement and cooling of the
562 igneous intrusions in the area. Reaction of feldspar to form böhmite and kaolinite was also performed by Fu et
563 al. (2009) on perthitic alkali feldspars under acidic hydrothermal conditions. Fu et al. (2009) noted the albite
564 (Na- feldspar) component reacted preferentially, which conforms to the observation in Figure 12 and supports
565 the Na depletion observed in sample NG29 (Fig. 13). The reactions between CO₂ and plagioclase provide an
566 important natural analogue to processes under investigation relevant to industrial CO₂ sequestration (e.g, Matter
567 et al. 2007; Matter and Kelemen 2009; Matter et al. 2016) and demonstrate how natural releases of CO₂ from
568 igneous activity in sedimentary basins can be naturally moderated (e.g, Jones et al. 2016).

569

CONTROLS ON FLUID FLOW

570 Inasmuch as Type 2 diagenesis is a result of fluid flux and Type 1 diagenesis is a result of absence of this flux, it
571 is logical to conclude that the enveloping lithology (lava) is responsible for compartmentalizing either individual
572 dunes or volumes of rock encompassing dunes. If we consider that the lava is completely impermeable (which is
573 unrealistic), it would also be logical to infer that fracture connectivity (i.e, faults and joints) controls fluid flow
574 and some dunes are simply part of this fracture network and others have not been intersected. However, lava
575 piles are not impermeable (e.g, Saar and Manga 1999); indeed, they can be major conductors of subsurface
576 fluids, such as in the Columbia River Basalts, where the major aquifers are basalt (Newcomb 1961; see also
577 Saar and Manga 1999), as well as in thick basaltic sequences offshore where high permeability can be preserved
578 within flow tops (e.g, Millett et al. 2016). Permeability in pahoehoe lava flows is generally highest within the
579 highly vesicular upper and lower crusts; the massive central lava cores show typically low permeability to
580 nearly impermeable layers (Newcomb 1961; Smith 2004), where any permeability is restricted to cooling
581 fractures (e.g, Petford 2003) or on the grain scale through alteration. A lava sequence can therefore be
582 considered as having the potential to show markedly different porosity/permeability, with higher permeability
583 layers running along lava flow tops (e.g, Millett et al., 2016).

584 The lowermost Tafelkop-type lava flows exhibit a compound-braided facies nature and do not form thick tabular
585 sheets (Jerram 2002). Such lava flows have markedly higher crust-to core-ratios (e.g, Nelson et al. 2009) and
586 contain abundant vesicles and fractures. The compound nature of these Tafelkop-type lavas in Dune Valley,
587 combined with the visible occurrence of highly vesicular zones, suggests that the lava was, at least partially
588 permeable in the horizontal direction. The stacking of many compound pahoehoe lava flows with relatively
589 permeable crusts and relatively impermeable cores would have resulted in a complex permeable network,
590 incapable of isolating dunes from fluid flow alone. Another element must be responsible for the
591 compartmentalization; we propose this to be the igneous dikes in the area. This hypothesis is supported by field
592 relationships in Dune C (Figs. 3, 16) where the dune is crosscut by an ~ 4 m-thick dolerite dike. An
593 impermeable contact zone is developed where the dike intersects the sandstone (similar to the hot type 3
594 diagenesis). The dike separates red Type 1 sand from white Type 2 sand. The dike follows the same ~ N-S trend
595 as most dikes in the Huab Outliers. Some dikes pass into and feed the lower Tafelkop lava (e.g, Jerram et al.
596 1999a) while others fed lavas that were younger than the youngest exposed lavas in the region, and can be seen
597 cutting up through the whole preserved sequence. Although it is possible that dike pathways are weaknesses that
598 can be reused by later phases of dike intrusion, the information from the dikes in the Huab Outliers suggests that
599 the timing and depth of compartment formation (igneous intrusion) could be from as little as 300 m of burial
600 (e.g, the feeder dikes) up to the complete thickness of the volcanic pile.

601 Fractures are irregular and poorly expressed in the Tafelkop basalt lavas due to the intense desert weathering,
602 but fractures would have formed during cooling and possibly subsequent tectonic activity. The presence of open
603 fractures and fissures is indirectly preserved due to sand infill (e.g, Jerram et al., 2000a; Jerram and Stollhofen
604 2002), creating molds of the fracture cavities. N-S-trending low-displacement faults (centimeters) frequently
605 cross cut sandstone beds in Dune Valley (Fig. 16), but they have not been found separating Type 1 sand from
606 Type 2 sand. Faults are frequently mineralized with calcite (also isotopically Type 2 affinity), and, depending on
607 timing, may have been pathways for the flow of diagenetic fluids. The relative timings of the diagenetic types is
608 presented in Figure 17, which highlights that Type 3 is restricted to lava flow (and in some cases dike
609 emplacement) during the volcanism, as these are “hot” contacts of the sand with the lava. The Type 1 and 2
610 diagenesis occurring largely during the later stages of synvolcanic burial and further burial of the sequence (Fig.
611 17).

612 A conceptual model of fluid flow in the basalt pile is given in Figure 18, to help explain the distribution and
 613 compartmentalization of the Type 2 diagenesis. It is proposed that in the Tafelkop lavas, vertical to subvertical
 614 igneous intrusions are largely responsible for isolating red dunes from diagenetic fluids (Fig. 18). The use of the
 615 Type 2 sandstone as a tracer of fluid flow compartmentalized in a mixed basalt-siliciclastic system has identified
 616 igneous dikes as the compartment-forming component, not the lava flows. This in part confirms the notion that
 617 the dike system is acting as both a barrier laterally and modifying the permeability pathways of fluid flow (e.g.,
 618 Schofield et al., 2015; Senger et al., 2017). The exploitation of similar mixed-lithology hydrocarbon plays in
 619 volcanic margins should consider the possible hydraulic connectivity of compound lava flows and sandstones
 620 (e.g, the Faroe-Shetland basin and offshore Namibia), and be prepared to encounter dike-compartmentalized
 621 reservoirs affecting charge and migration as well as the field development design required.

622

IMPLICATIONS AND CONCLUSIONS

- 623 1. Hot contacts at the bases of newly emplaced lava flows show a marked reduction in porosity and
 624 permeability (Table 1, Fig. 9), as a result of rapid mechanical compaction of unconsolidated sand,
 625 dissolution associated with hydrothermal activity generated by the degassing hot lava above, and
 626 associated cementation. This “indurated” zone occurs a few tens of centimeters below these contacts,
 627 resulting in the Type 3 diagenesis (Fig. 17).
- 628 2. Later fluid flow traced through inter-basalt sediments has been found to be heterogeneous and
 629 controlled by igneous dike intrusions (e.g, Figs. 16, 18), some isolated sediment bodies being
 630 connected to the flow regime, and some apparently isolated. The implication is that any fluid could be
 631 controlled in this manner, including hydrocarbons. In the case in question, the Type 2 diagenesis
 632 affected approximately half of the dunes exposed in Dune Valley, though the precise volume of
 633 sandstone affected is not known.
- 634 3. These findings suggest that volume estimates of sediment-lava interbedded reservoirs (for petroleum
 635 exploration), where encountered in the subsurface, should take into account that not all sediment bodies
 636 predicted in similar situations will be charged with hydrocarbons, despite sharing stratigraphical
 637 location, depositional environment and geological structure.
- 638 4. The Dune Valley outcrops of white sandstone have been identified as a natural analogue to the
 639 proposed carbon sequestration method of Hangx and Spiers (2009); in our case magmatic CO₂ is being
 640 sequestered. Our findings have implications for the total amount of CO₂ thought to have been emitted

641 from large igneous provinces (e.g. The Paraná-Etendeka or the Deccan Traps). Such estimates should
642 account for CO₂ that is sequestered within sediments in hydraulic connection with the igneous
643 province (e.g. Caldeira and Ramoino 1990; Wignall 2001; McHone 2003; Jones et al. 2016) as well as
644 within the igneous rock themselves (Matter et al. 2016).

645 5. Apart from the tracing of heterogeneous hydrothermal fluid flow through the basalt pile, the results of
646 Type 2 diagenesis left reduced porosity and permeability compartments (the white sandstone), which
647 do not relate to depositional environment or geological structure. These poorer potential reservoir rocks
648 are connected to the fluid migration pathways, whereas the better-reservoir-quality red sandstones are
649 not (at least at the time of hydrothermal activity). This dichotomy should be appreciated if similar rocks
650 are encountered during exploration in volcanic provinces. For instance, development of mixed basalt-
651 siliciclastic reservoirs (such as Rosebank) should not expect all stratigraphically trapped sandstone
652 units in the play to show identical diagenesis, and hence reservoir properties. Conversely, if exploration
653 drilling encounters poor-quality sandstone, with evidence of Type 2 diagenesis, it should be considered
654 that good-quality sandstone may exist in close proximity.

655 **ACKNOWLEDGMENTS**

656 We would like to thank the VMRC partners (Chevron, ENI, DONG, Statoil, OMV and HESS) and
657 OneNortheast (sponsored by Rick Smith, FWS Consultants) for funding this project. This work was also partly
658 supported by the Research Council of Norway through its Centers of Excellence funding scheme, project
659 number 223272 (CEED). We would like to thank Joanna Garland of Cambridge Carbonates Ltd. who provided
660 valuable feedback during the final preparation of the manuscript. We thank Andrew Hurst and Colin Taylor
661 (Aberdeen) and Nicholas Odling (Edinburgh) for facilitating laboratory work. Breno Waichel (and Brazilian
662 colleagues), Tim Watton, Sam Clark, Alex Baker, Kevin Purvis and Victoria Gee are thanked for help and
663 guidance. Gabi Schneider and the staff at the Geological Survey of Namibia are thanked for their continued
664 support in Namibia. We thank Sally Sutton, Nick Schofield, and an anonymous reviewer for thoughtful
665 comments. Leslie Melim is thanked for editorial guidance and John Southard is thanked for detailed technical
666 edits; they have significantly improved the manuscript, especially regarding organization.

667 **REFERENCES**

668 Arnórsson, S., 1986, Chemistry of gases associated with geothermal activity and volcanism in Iceland: A
669 review: *Journal of Geophysical Research: Solid Earth*, v. 91, p. 12261-12268.

- 670 Angkasa, S.S., Jerram, D.A., Millett, J.M., Svensen, H.H., Planke, S., Taylor, R.A., Schofield, N. and Howell,
671 J., 2017, Mafic intrusions, hydrothermal venting, and the basalt-sediment transition: Linking onshore and
672 offshore examples from the North Atlantic igneous province: *Interpretation*, v.5(3), SK83-SK101.
- 673 Beitler, B., Chan, M., and Parry, W., 2003, Bleaching of Jurassic Navajo sandstone on Colorado Plateau
674 Laramide highs: Evidence of exhumed hydrocarbon supergiants?: *Geology*, v. 31, p. 1041-1044.
- 675 Beitler, B., Parry, W., and Chan, M., 2005, Fingerprints of fluid flow: chemical diagenetic history of the Jurassic
676 Navajo Sandstone, southern Utah, USA: *Journal of Sedimentary Research*, v. 75, p. 547-561.
- 677 Beswetherick, S., Miglio, G., Ross, A., and Poynter, S., 2009, The Ann-Marie Prospect, Licence 005. Faroe
678 Islands Exploration Conference: Proceedings of the 2nd Conference. *Annales Societatis Scientiarum Færoensis*,
679 Supplementum, v. 50, p. 246-266.
- 680 Bowen, G.J., and Wilkinson, B., 2002, Spatial distribution of $\delta^{18}\text{O}$ in meteoric precipitation: *Geology*, v. 30, p.
681 315-318.
- 682 Brownlow, A.H., 1996, *Geochemistry: Upper Saddle River, New Jersey*, Prentice Hall, 580 p.
- 683 Bryan, S.E., Ukstins Peate, I., Peate, D.W., Self, S., Jerram, D.A., Mawby, M.R., Marsh, J.S., and Miller, J.A.,
684 2010, The largest volcanic eruptions on Earth: *Earth-Science Reviews*, v. 102(3), p. 207-229.
- 685 Cai, W., Yu, J., Cheng, B., Su, B.L., and Jaroniec, M., 2009, Synthesis of boehmite hollow core/shell and
686 hollow microspheres via sodium tartrate-mediated phase transformation and their enhanced adsorption
687 performance in water treatment: *Journal of Physical Chemistry C*, v. 113, p. 14,739-14,746.
- 688 Caldeira, K., and Rampino, M.R., 1990, Carbon dioxide emissions from Deccan volcanism and a K/T boundary
689 greenhouse effect: *Geophysical Research Letters*, v. 17, p. 1299-1302.
- 690 Candy, I., Adamson, K., Gallant, C.E., Whitfield, E., and Pope, R., 2012, Oxygen and carbon isotopic
691 composition of Quaternary meteoric carbonates from western and southern Europe: Their role in
692 palaeoenvironmental reconstruction: *Palaeogeography, Palaeoclimatology, Palaeoecology*, v. 326-328, p. 1-11.
- 693 Chan, M.A., Parry, W.T., and Bowman, J.R., 2000, Diagenetic hematite and manganese oxides and fault-related
694 fluid flow in Jurassic sandstones, Southeastern Utah: *AAPG, Bulletin*, v. 84, p. 1281-1310.
- 695 Clemson, J., Cartwright, J., and Booth, J., 1997, Structural segmentation and the influence of basement structure
696 on the Namibian passive margin: *Geological Society of London, Journal*, v. 154, p. 477-482.
- 697 Davison, I., 1999, Tectonics and hydrocarbon distribution along the Brazilian South Atlantic margin, *in*
698 Cameron, N.R., Bate, R.H., and Clure, V.S., eds., *The oil and gas habitats of the South Atlantic: Geological*
699 *Society, London, Special Publication*, v. 153, p. 133-151.

- 700 Delmelle, P., and Stix., 2000, Volcanic gases, *in* Sigurdsson, H. et al., eds., *Encyclopaedia of Volcanoes*:
701 Academic press, p. 803-145.
- 702 Dias, Á.S., Früh-Green, G. L., Bernasconi, S. M., and Barriga, F.J.A.S, 2011, Geochemistry and stable isotope
703 constraints on high-temperature activity from sediment cores of the Saldanha hydrothermal field: *Marine*
704 *Geology*, v. 279, p. 128-140.
- 705 Dickinson, W., and Milliken, K., 1995, The diagenetic role of brittle deformation in compaction and pressure
706 solution, Etjo sandstone, Namibia: *The Journal of Geology*, v. 103, p. 339-347.
- 707 Dodd, S.C., Niocaill, C.M., and Muxworthy, A.R., 2015, Long duration (>4 Ma) and steady-state volcanic
708 activity in the early Cretaceous Paraná–Etendeka Large Igneous Province: New palaeomagnetic data from
709 Namibia: *Earth and Planetary Science Letters*, v. 414, p. 16-29.
- 710 Duncan, A.R., Newton, S.R., van den Berg, C., and Reid, D.L., 1989, Geochemistry and petrology of dolerite
711 sills in the Huab River Valley, Damaraland, north-western Namibia: *Geological Survey of Namibia,*
712 *Communications*, v. 5, p. 5-18.
- 713 Folk, R.L., 1976, Reddening of desert sands: Simpson Desert, NT, Australia: *Journal of Sedimentary Petrology*,
714 v. 46, p. 604-615.
- 715 França, A., Araújo, L., Maynard, J., and Potter, P., 2003, Secondary porosity formed by deep meteoric leaching:
716 Botucatu eolianite, southern South America: *AAPG, bulletin*, v. 87, p. 1073-1082.
- 717 Fu, Q., Lu, P., Konishi, H., Dilmore, R., Xu, H., Seyfried, W.E. Jr., and Zhu, C., 2009, Coupled alkali-feldspar
718 dissolution and secondary mineral precipitation in batch systems: 1. New experiments at 200 °C and 300 bars:
719 *Chemical Geology*, v. 258, p. 125-135.
- 720 Garden, I.R., Guscott, S.C., Burley, S.D., Foxford, K.A., Walsh, J.J., and Marshall, J, 2001, An exhumed
721 palaeo-hydrocarbon migration fairway in a faulted carrier system, Entrada Sandstone of SE Utah, USA:
722 *Geofluids*, v. 1, p. 195-213.
- 723 Gierlowski-Kordesch, E.H., Weismiller, H.C., Stigall, A.L., and Hembree, D.I., 2015, Pedogenic mud
724 aggregates and sedimentation patterns between basalt flows (Jurassic Kalkrand Formation, Namibia), *in* Larsen,
725 D., Egenhoff, S.O., and Fishman, N.S., eds., *Paying Attention to Mudrocks: Priceless!*: Geological Society
726 of America Special Paper 515, p. 65–86.
- 727 Gilg, H.A., Morteani, G., Kostitsyn, Y., Preinfalk, C., Gatter, I., and Strieder, A.J, 2003, Genesis of amythyst
728 geodes in basaltic rocs of the Serra Geral Formation (Ametista do Sul, Rio Grande do Sul, Brazil): a fluid

- 729 inclusion, REE, oxygen, carbon, and Sr study on basalt, quartz and calcite: *Mineralium Deposita*, v. 38, p. 1009-
730 1025.
- 731 Goudie, A.S., and Eckardt, F., 1999, The evolution of the morphological framework of the central Namib
732 Desert, Namibia, since the Early Cretaceous: *Geografiska Annaler, Series A, Physical Geography*, p. 81, v. 443-
733 458.
- 734 Grove, C., and Jerram, D.A., 2011, jPOR: An ImageJ macro to quantify total optical porosity from blue-stained
735 thin sections: *Computers & Geosciences*, v. 37, p. 1850-1859.
- 736 Hangx, S.J.T., and Spiers, C.J., 2009, Reaction of plagioclase feldspars with CO₂ under hydrothermal
737 conditions: *Chemical Geology*, v. 265, p. 88-98.
- 738 Hazewinkel, M., ed., 2001, "Student test": *Encyclopedia of Mathematics*, Springer, ISBN 978-1-55608-010-4
- 739 Helland-Hansen, D., 2009, Rosebank – Challenges to development from a subsurface perspective: *Faroe Islands*
740 *Exploration Conference: Proceedings of the 2nd Conference: Annales Societatis Scientiarum Færoensis*,
741 *Supplementum*, v. 50, p. 241-245.
- 742 Henley, R.W., and Ellis, A.J., 1983, Geothermal systems ancient and modern: a geochemical review: *Earth-*
743 *Science Reviews*, v. 19, p. 1-50.
- 744 Hitchen, K., Johnson, H., and Gatliff, R.W., eds., 2013, *Geology of the Rockall Basin and Adjacent Areas*:
745 *British Geological Survey*, Keyworth, Nottingham, UK, 193 p.
- 746 Horsthemke, E., Ledendeker, S., and Porada, H., 1990, Depositional environments and stratigraphic correlation
747 of the Karoo Sequence in northwestern Damaraland: *Geological Survey of Namibia, Communications*, v. 6, p.
748 63-73.
- 749 Horton, T.W., Atkinson, L., and Oze, C., 2012, Hydrothermal carbonate geochemistry of the Ngatamariki
750 subsurface reservoir, New Zealand: *Proceedings of the Thirty-Seventh Workshop on Geothermal Reservoir*
751 *Engineering*, Stanford, California, p. 1-8.
- 752 Howell, J., and Mountney, N., 2001, Aeolian grain flow architecture: hard data for reservoir models and
753 implications for red bed sequence stratigraphy: *Petroleum Geoscience*, v. 7, p. 51-56.
- 754 Hurst, A., and Goggin, D., 1995, Probe permeametry: An overview and bibliography: *AAPG, bulletin*, v. 79, p.
755 463-463.
- 756 Jerram, D.A., Mountney, N., Holzförster, F., and Stollhofen, H., 1999a, Internal stratigraphic relationships in the
757 Etendeka Group in the Huab Basin, NW Namibia: understanding the onset of flood volcanism: *Journal of*
758 *Geodynamics*, v. 28, p. 393-418.

- 759 Jerram, D.A., Mountney, N., and Stollhofen, H., 1999b, Facies architecture of the Etjo Sandstone Formation and
760 its interaction with the Basal Etendeka Flood Basalts of northwest Namibia: implications for offshore
761 prospectivity *in* Cameron, N.R., Bate, R.H., and Clure, V.S., eds., The oil and gas habitats of the South Atlantic
762 Geological Society, London, Special Publication, v. 153, p. 367-380.
- 763 Jerram, D.A., Mountney, N., Howell, J., Long, D., and Stollhofen, H., 2000a, Death of a sand sea: an active
764 aeolian erg systematically buried by the Etendeka flood basalts of NW Namibia: Geological Society of London,
765 Journal, v. 157, p. 513-516.
- 766 Jerram, D.A., Mountney, N., Howell, J., and Stollhofen, H., 2000b, The Fossilised Desert: recent developments
767 in our understanding of the Lower Cretaceous deposits in the Huab Basin, NW Namibia: Geological Survey of
768 Namibia, Communications, v. 12, p. 269-278.
- 769 Jerram, D.A., and Robbe, O., 2001, Building a 3-D geologic model of a flood basalt: an example from the
770 Etendeka, NW Namibia: Visual Geosciences, v. 6, p.1-8.
- 771 Jerram, D.A., 2002, Volcanology and faces architecture of flood basalts: Volcanic Rifted Margins, v. 362, p.
772 119.
- 773 Jerram, D.A., and Stollhofen, H., 2002, Lava–sediment interaction in desert settings: are all peperite-like
774 textures the result of magma–water interaction?: Journal of Volcanology and Geothermal Research, v. 114, p.
775 231-249.
- 776 Jerram, D.A., and Widdowson, M., 2005, The anatomy of Continental Flood Basalt Provinces: geological
777 constraints on the processes and products of flood volcanism: Lithos, v. 79, p. 385-405.
- 778 Jones, M.T., Jerram, D.A., Svensen, H., and Grove, C., 2016, The effects of large igneous provinces on the
779 global carbon and sulphur cycles: Palaeogeography, Palaeoclimatology, Palaeoecology, v. 441, p. 4-21.
- 780 Jungslager, E.H.A., 1999, Petroleum habitats of the Atlantic margin of South Africa prospectivity *in* Cameron,
781 N.R., Bate, R.H., and Clure, V.S., eds., The oil and gas habitats of the South Atlantic Geological Society,
782 London, Special Publication, v. 153 p. 153-168.
- 783 King, D.W., 1998, Role of carbonate speciation on the oxidation rate of Fe(II) in aquatic systems:
784 Environmental Science & Technology, v. 32, p. 2997-3003.
- 785 Kirkland, D.W., Denison, R.E., and Rooney, M.A., 1995, Diagenetic alteration of Permian strata at oil fields of
786 south central Oklahoma, USA: Marine and Petroleum Geology, v. 12, p. 629-644.
- 787 Lowenstern, J., 2001, Carbon dioxide in magmas and implications for hydrothermal systems: Mineralium
788 Deposita, v. 36, p. 490-502.

- 789 Lundegard, P.D., 1992, Sandstone porosity loss: a "big picture" view of the importance of compaction: *Journal*
790 *of Sedimentary Petrology*, v. 62, p. 250-260.
- 791 Ma, Y., Liu, C., Zhao, J., Huang, L., Yu, L., and Wang, J., 2007, Characteristics of bleaching of sandstone in
792 northeast of Ordos Basin and its relationship with natural gas leakage: *Science in China Series D: Earth*
793 *Sciences*, v. 50, p. 153-164.
- 794 Matter, J.M., Takahashi, T., and Goldberg, D., 2007, Experimental evaluation of in situ CO₂-water-rock
795 reactions during CO₂ injection in basaltic rocks: Implications for geological CO₂ sequestration: *Geochemistry,*
796 *Geophysics, Geosystems*, v. 8, No. 2.
- 797 Matter, J.M., and Kelemen, P.B., 2009, Permanent storage of carbon dioxide in geological reservoirs by mineral
798 carbonation: *Nature Geoscience*, v. 2, p. 837-841.
- 799 Matter, J.M., Stute, M., Snæbjörnsdóttir, S.Ó., Oelkers, E.H., Gislason, S.R., Aradóttir, E.S., Sigfusson, B.,
800 Gunnarsson, I., Sigurdardóttir, H., Gunnlaugsson, E., and Axelsson, G., 2016, Rapid carbon mineralization for
801 permanent disposal of anthropogenic carbon dioxide emissions: *Science*, v. 352(6291), p. 1312-1314.
- 802 Marsh, J.S., Erlank, A.J., and Duncan, A.R., 1991, Preliminary geochemical data for dolerite dykes and sills of
803 the southern part of the Etendeka Igneous Province: *Geological Survey of Namibia, Communications*, v. 7, p.
804 71-74.
- 805 Marsh, J.S., Ewart, A., Milner, S., Duncan, A., and Miller, R., 2001, The Etendeka Igneous Province: magma
806 types and their stratigraphic distribution with implications for the evolution of the Parana-Etendeka flood basalt
807 province: *Bulletin of Volcanology*, v. 62, p. 464-486.
- 808 Marx, V.L., 2009, Impacts of upstream uses on the alluvial aquifer of the Swakop River, Namibia
809 [Diplomarbeit]: Albert Ludwig Universität Freiburg, Germany, 85 p.
- 810 McHone, J.G., 2003, Volatile emissions from central Atlantic magmatic province basalts: mass assumptions and
811 environmental consequences: *American Geophysical Union, Geophysical Monograph*, v. 136, p. 241-254.
- 812 McLachlan, I.R., 1990, Introductory note on the history of the Kudu prospect: *Geological Survey of Namibia,*
813 *Communications*, v. 6, p. 5.
- 814 Millett, J.M., Wilkins, A.D., Campbell, E., Hole, M.J., Taylor, R.A., Healy, D., Jerram, D.A., Jolley, D.W.,
815 Planke, S., Archer, S.G. and Blischke, A., 2016, The geology of offshore drilling through basalt sequences:
816 Understanding operational complications to improve efficiency: *Marine and Petroleum Geology*, v. 77, p. 1177-
817 1192.

- 818 Milner, S., Duncan, A., Whittingham, A., and Ewart, A., 1995, Trans-Atlantic correlation of eruptive sequences
819 and individual silicic volcanic units within the Paraná-Etendeka igneous province: *Journal of Volcanology and*
820 *Geothermal Research*, v. 69, p. 137-157.
- 821 Moulton, G.F., 1926, Some features of redbed bleaching: *AAPG, bulletin*, v. 10, p. 304-311.
- 822 Mountney, N., Howell, J., Flint, S., and Jerram, D., 1998, Aeolian and alluvial deposition within the Mesozoic
823 Etjo Sandstone Formation, northwest Namibia: *Journal of African Earth Sciences*, v. 27, p. 175-192.
- 824 Mountney, N., Howell, J., Flint, S., and Jerram, D., 1999a, Relating eolian bounding-surface geometries to the
825 bed forms that generated them: Etjo Formation, Cretaceous, Namibia: *Geology*, v. 27, p. 159.
- 826 Mountney, N., Howell, J., Flint, S., and Jerram, D., 1999b, Climate, sediment supply and tectonics as controls
827 on the deposition and preservation of the aeolian-fluvial Etjo Sandstone Formation, Namibia: *Geological*
828 *Society of London, Journal*, v. 156, p. 771-777.
- 829 Naylor, H., Turner, P., Vaughan, D.J., and Fallick, A.E., 1989, The Cherty Rock: a petrographic and isotopic
830 study of a Permo Triassic calcrete: *Geological Journal*, v. 24, p. 205-221.
- 831 Nelson, C., Jerram, D., and Hobbs, R., 2009, Flood basalt facies from borehole data: implications for
832 prospectivity and volcanology in volcanic rifted margins: *Petroleum Geoscience*, v. 15, p. 313-324.
- 833 Newcomb, R.C., 1961, Storage of ground water behind subsurface dams in the Columbia River Basalt,
834 Washington, Oregon, and Idaho: *Geological Survey Professional Paper*, 383-A, Washington, US Government
835 Printing Office.
- 836 O'Neil, J.R., Clayton, R.N., and Mayeda, T.K., 1969, Oxygen isotope fractionation in divalent metal carbonates:
837 *Journal of Chemical Physics*, v. 51, p. 5547-5558.
- 838 Parry, W., Chan, M., and Beitler, B., 2004, Chemical bleaching indicates episodes of fluid flow in deformation
839 bands in sandstone: *AAPG, bulletin*, v. 88, p. 175-191.
- 840 Peate, D., 1997, The Paraná-Etendeka Province: *American Geophysical Union, Geophysical Monograph*, v.
841 100, p. 217-246.
- 842 Peate, I.U., Larsen, M., and Leshner, C.E., 2003, The transition from sedimentation to flood volcanism in the
843 Kangerlussuaq Basin, East Greenland: basaltic pyroclastic volcanism during initial Palaeogene continental
844 break-up: *Geological Society of London, Journal*, v. 160, p. 759-772.
- 845 Petford, N., 2003, Controls on primary porosity and permeability development in igneous rocks *in* Petford, N.,
846 and McCaffrey, K.J.W., eds., *Hydrocarbons in Crystalline Rocks*: *Geological Society of London, Special*
847 *Publication*, v. 214, p. 93-107.

- 848 Petry, K., Jerram, D.A., del Pilar M, de Almeida, D., and Zerfass, H., 2007, Volcanic-sedimentary features in
849 the Serra Geral Fm. Paraná Basin, southern Brazil: examples of dynamic lava-sediment interactions in an arid
850 setting: *Journal of Volcanology and Geothermal Research*, v. 159, p. 313-325.
- 851 Platt, J.D., 1994, Geochemical evolution of pore waters in the Rotliegend (Early Permian) of northern Germany:
852 *Marine and Petroleum Geology*, v. 11, p. 66-78.
- 853 Purvis, K., and Wright, V.P, 1991, Calcretes related to phreatophytic vegetation from the Middle Triassic Otter
854 Sandstone of South West England: *Sedimentology*, v. 88, p. 539-551.
- 855 Raab, M., Brown, R., Gallagher, K., Weber, K., and Gleadow, A., 2005, Denudational and thermal history of the
856 Early Cretaceous Brandberg and Okenyenya igneous complexes on Namibia's Atlantic passive margin:
857 *Tectonics*, v. 24, No. 3.
- 858 Rateau, R., Schofield, N., and Smith, M., 2013, The potential role of igneous intrusions on hydrocarbon
859 migration, West of Shetland: *Petroleum Geoscience*, v. 19, p. 259-272.
- 860 Rollinson, H.R., 1993, *Using Geochemical Data; Evaluation, Eresentation, Interpretation*: Harlow, Pearson
861 Education, 352 p.
- 862 Ross, P.S., Ukstins Peate, I., McClintock, M., Xu, Y., Skilling, I., White, J., and Houghton, B., 2005, Mafic
863 volcanoclastic deposits in flood basalt provinces: a review: *Journal of volcanology and Geothermal Research*, v.
864 145, p. 281-314.
- 865 Rye, R.O., 2005, A review of the stable-isotope geochemistry of sulfate minerals in selected igneous
866 environments and related hydrothermal systems: *Chemical Geology*, v. 215, p. 5-36.
- 867 Saar, M., and Manga, M., 1999, Permeability-porosity relationship in vesicular basalts: *Geophysical Research*
868 *Letters*, v. 26, p. 111-114.
- 869 Schofield, N., and Jolley, D.W., 2013, Development of intra-basaltic lava-field drainage systems within the
870 Faroe-Shetland Basin: *Petroleum Geoscience*. v. 19, p. 273-288.
- 871 Schofield, N., Holford, S., Millett, J., Brown, D., Jolley, D., Passey, S.R., Muirhead, D., Grove, C., Magee, C.,
872 Murray, J., Hole, M., Jackson, C.A.-L., and Stevenson, C., 2015, Regional magma plumbing and emplacement
873 mechanisms of the Faroe-Shetland Sill Complex: implications for magma transport and petroleum systems
874 within sedimentary basins: *Basin Research*, v. 29, p. 41-63.
- 875 Schreiber, U.M., 2006, *Geological Map of Namibia 1: 250 000 Geological Series, Sheet 2014 – Fransfontein*
876 (Provisional): Geological Survey of Namibia.

- 877 Scherer, C., 2002, Preservation of aeolian genetic units by lava flows in the Lower Cretaceous of the Paraná
878 Basin, southern Brazil: *Sedimentology*, v. 49, p. 97-116.
- 879 Scherer, C.M.S., and Goldberg, K., 2007, Palaeowind patterns during the latest Jurassic- earliest Cretaceous in
880 Gondwana: evidence from aeolian cross strata of the Botucatu Formation, Brazil: *Palaeogeography*,
881 *Palaeoclimatology, Palaeoecology*, v. 248, p. 1-10.
- 882 Schöner, R., and Gaupp, R., 2005, Contrasting red bed diagenesis: the southern and northern margin of the
883 Central European Basin: *International Journal of Earth Sciences*, v. 94, p. 897-916.
- 884 Schutter, S.R., 2003, Hydrocarbon occurrence and exploration in and around igneous rocks *in* Petford, N., and
885 McCaffrey, K.J.W., eds., *Hydrocarbons in Crystalline Rocks: Geological Society of London, Special*
886 *Publication*, v. 214, p. 7-33.
- 887 Scotese, C.R., 2001, *Atlas of Earth History, Volume 1, Palaeogeography: PALEOMAP Project*, Arlington,
888 Texas, 52 p.
- 889 Self, S., Keszthelyi, L., and Thordarson, T., 1998, The importance of pahoehoe: *Annual Review of Earth and*
890 *Planetary Sciences*, v. 26, p. 81-110.
- 891 Senger, K., Millett, J., Planke, S., Ogata, K., Eide, C.H., Festøy, M., Galland, O., and Jerram, D.A., 2017,
892 *Effects of igneous intrusions on the petroleum system: a review: First Break*, v. 35, no. 6, p. 47-56.
- 893 Shevenell, L., and Goff, F., 1993, Addition of magmatic volatiles into the hot spring waters of Loowit Canyon,
894 Mount St. Helens, Washington, USA: *Bulletin of Volcanology*, v. 55, p. 489-503.
- 895 Simmons, S., and Christenson, B., 1994, Origins of calcite in a boiling geothermal system: *American Journal of*
896 *Science*, v. 294, p. 361-400.
- 897 Smallwood, J.R., Prescott, D., and Kirk, W., 2004, Alternatives in Paleocene exploration West of Shetland: a
898 case study: *Scottish Journal of Geology*, v. 40, p. 131-143.
- 899 Smith, R.P., 2004, Geologic setting of the Snake River Plain Aquifer and vadose zone: *Vadose Zone Journal*, v.
900 3, no. 1, p. 47-58.
- 901 Solomons, W., Goudie, A., and Mook, W.G., 1978, Isotopic composition of calcrete deposits from Europe,
902 Africa and India: *Earth Surface Processes*, v. 3, p. 43-57.
- 903 Stanistreet, I., and Stollhofen, H., 1999, Onshore equivalents of the main Kudu gas reservoir in Namibia *in*
904 Cameron, N.R., Bate, R.H., and Clure, V.S., eds., *The oil and gas habitats of the South Atlantic: Geological*
905 *Society of London, Special Publication*, v. 153, p. 345-365.

- 906 Stevens, T.O., and McKinley, J.P., 2000, Abiotic controls on H₂ production from basalt-water reactions and
 907 implications for aquifer biogeochemistry: *Environmental science & technology*, v. 34, p. 826-831.
- 908 Surdam, R.C., Jiao, Z.S., and MacGowan, D.B., 1993, Redox reactions involving hydrocarbons and mineral
 909 oxidants: A mechanism for significant porosity enhancement in sandstones: *AAPG, bulletin*, v. 77, p. 1509-
 910 1518.
- 911 Waichel, B.L., Scherer, C., and Frank, H.T., 2008, Basaltic lava flows covering active aeolian dunes in the
 912 Paraná Basin in southern Brazil: Features and emplacement aspects: *Journal of Volcanology and Geothermal
 913 Research*, v. 171, p. 59-72.
- 914 Waichel, B.L., de Lima, E.F., Viana, A.R., Scherer, C.M., Bueno, G.V., and Dutra, G., 2011, Stratigraphy and
 915 volcanic facies architecture of the Torres Syncline, Southern Brazil, and its role in understanding the Paraná-
 916 Etendeka Continental Flood Basalt Province: *Journal of Volcanology and Geothermal Research*, v. 215, p. 74-
 917 82.
- 918 Watton, T.J., Cannon, S., Brown, R.J., Jerram, D.A., and Waichel, B.L., 2014, Using formation micro-imaging,
 919 wireline logs and onshore analogues to distinguish volcanic lithofacies in boreholes: examples from Palaeogene
 920 successions in the Faroe-Shetland Basin, NE Atlantic *in* Cannon, S.J.C., and Ellis, D., eds., *Hydrocarbon
 921 Exploration to Exploitation West of Shetlands: Geological Society of London, Special Publication*, v. 397, p.
 922 173-192.
- 923 Walker, G.P.L., 1971, Compound and simple lava flows and flood basalts: *Bulletin of Volcanology*, v. 35, p.
 924 579-590.
- 925 White, D., 1957, Thermal waters of volcanic origin: *Geological Society of America, Bulletin*, v. 68, p. 1637.
- 926 Wignall, P.B., 2001, Large igneous provinces and mass extinctions: *Earth-Science Reviews*, v. 53, p. 1-33.
- 927 Wu, X., Zhang, B., Wang, D., and Hu, Z., 2012, Morphology evolution studies of boehmite hollow
 928 microspheres synthesized under hydrothermal conditions: *Materials Letters*, v. 70, p. 128-131.
- 929
- 930
- 931
- 932 Fig. 1. A) Location of Namibia in southern Africa. B) Distribution of Lower Cretaceous subaerial outcrop in
 933 Namibia (sediments and lava flows). Sediments are predominantly the Twyfelfontein Formation sandstones and
 934 lavas Paraná-Etendeka basalts, basaltic andesites, and silicic rhyolites. Huab outliers in red box. C)
 935 Cretaceous subaerial outcrop (sediments and lava flows) in the Huab Outliers. Dune valley in yellow box. Maps

936 compiled from own field mapping, Landsat 7 ETM+ imagery and maps published by the Geological Survey of
 937 Namibia.

938

939 Fig. 2. Stratigraphic succession of the Huab Basin (adapted from Jerram et al. 1999a). The units of interest form
 940 the upper parts of the Twyfelfountain Fm. and lower parts of the Awahab Fm. The relative distribution of
 941 Etendeka-related intrusions is also given (Kdo, green column). Note that the Awahab and Twyfelfountain Fms.
 942 are indicated as overlapping due to the interbedded nature of the sedimentary and igneous rocks.

943

944 Fig. 3. Geological map of Dune Valley. Barchnoid dunes detailed in this contribution are labelled (A, B, C).
 945 Point P and Q = origin of photographs in Fig. 5. The isolated nature of barchanoid dunes in the basaltic lava
 946 flows is evident from the map.

947

948 Fig. 4. Schematic diagram of passive drowning of Twyfelfontein erg system in the Huab Basin by Lower
 949 Cretaceous Basalts (mainly Tafelkop type basalts in Huab Outliers south of Huab River and a mix of Tafelkop
 950 and Tafelberg-type basalts along the main river sections). The transverse-draa-dominated major erg is first
 951 drowned (A), which restricts sediment mobility. Remaining unburied sediment is reworked to form minor erg
 952 (B) and bypass surfaces where sand infiltrates basalt cooling cracks but does not form dunes. The minor erg is
 953 then drowned by lava. Further lava drowning isolates more sediment from the active eolian system creating a
 954 sediment-poor eolian system of isolated barchanoid dunes (C), which are themselves drowned by lava.
 955 Successive drowning locks up more sediment until no more dunes are formed on lava surfaces (D). This is
 956 followed by differential diagenesis to form red and white sandstone. Drowning sequence is modified from
 957 Jerram et al. (1999a, 2000).

958

959 Fig. 5. A) Photograph of Dune Valley taken from the top of Awahab/Mikberg mountain (facing ~ SSW),
 960 numerous isolated dunes/sand bodies visible, completely preserved barchans dunes, Dune A (Type 3 white) and
 961 Dune B (Type 2 red) are labelled. B) Close-up of completely preserved barchan dune, with inset showing
 962 detailed measurements around the dune (adapted from Jerram et al. 2000a). C) Photograph of Dune B (facing

963 south from point Q Fig. 3), the contrasting sand color apparent together with equivalent stratigraphic level and
 964 proximity to each other. See Fig. 2 for stratigraphic labels.

965

966 Fig. 6. Geological map of Dune Valley showing a higher resolution of Dune A white and Dune B red sampled in
 967 this study. Contour spacing is 10 m, rock unit abbreviations are as in Fig. 2.

968 Table. 1. Average point-counting data for each “type” of diagenesis identified in this study. 500 points were
 969 counted for each sample (See also Grove and Jerram 2011).

970 Table. 2. Petrological and mineralogical comparison of contact sediments at Dune A white and Dune B red.

971 Table. 3. T-Test results of the point counting and permeability analysis of Type 1 red dunes and Type 2 white
 972 dunes (see table 2). All parameters other than opaque minerals have a T-Test result showing that the phase

973 counted is either statistically significantly different (95%) or highly statistically significantly different (99%).

974 The opaque-mineral result supports the hypothesis that iron oxides are reprecipitated locally as nodules. Highly
 975 statistically significant results are appended with an asterisk.

976 Fig. 7. Photomicrographs of sandstone at basalt contact for both white (sample NG26) and red (NG31) dunes to
 977 illustrate Type 3 diagenesis. A) NG26, white, shows increased compaction over the control, calcite cement,
 978 hematite grain coatings, and relatively unaltered feldspars (cf. Fig. 8). B) NG31, red, shows increased
 979 compaction over the control, calcite cement and hematite grain coatings. C) NG52, which is a control sample
 980 from major erg not in close proximity to igneous rocks; cementation and compaction are less than both samples
 981 at the contact with lava. No appreciable difference exists between Dune A (white) and Dune B (red) examples at
 982 the hot contacts, with the original porosity being occluded predominantly by calcite. K = potassium feldspar, Il
 983 = ilmenite, Calc = calcite, Haem = hematite.

984 Fig. 8. Photomicrographs of the white sandstone illustrating Type 2 diagenesis and comparing with red Type 1
 985 diagenesis. A) NG33 Dune B red 2 m below hot contact, connected pores, both K-spar and plagioclase detrital
 986 grains present. B, C) Dune A white 2 m below hot lava contact, kaolinite and calcite fills pores replacing
 987 plagioclase and some k-spar, which has enabled increased compaction. D, E) Dune A white, 3 m below hot lava
 988 contact, diagenetic assemblage is same as NG28, part E shows a plagioclase being transformed to kaolinite.

989 Thin sections stained for K-spar and carbonates. K = K-spar, calc = calcite, kao = kaolinite, q-og = quartz
 990 overgrowth, Haem = hematite, PPL = plane polarized Light, XPL = cross polarized light.

991 Fig. 9. A) Graph of porosity against distance from contact for Dune A (white), Dune B (red), and other isolated
 992 dunes in Dune Valley (white or red, see table 3). All porosities decrease toward hot contact, red dunes regain
 993 porosity more rapidly due to absence of secondary hydrothermal alteration (Type 2 diagenesis). Linear trend
 994 lines shown for Dune A white (blue) and Dune B red (red) both show good correlations with distance. B)
 995 Compaction-porosity loss (COPL) and cementation-porosity loss (CEPL) against distance below lava for Dune
 996 A (white), Dune B (red), and other isolated dunes in Dune Valley (white or red). COPL increases rapidly within
 997 30 cm of contact due to loading of lava on unconsolidated sediment combined with effects of corrosive volcanic
 998 gases on feldspar grains.

999 Fig. 10. A) Relationship between probe permeability (logarithmic scale) and distance below hot contact for red
 1000 and white dunes. Both types of permeability decrease in proximity to the contact zone, but white dunes do not
 1001 increase to equal levels of red dunes. Linear regression trends are shown for white Dune A (blue) and red Dune
 1002 B (red). B) Relationship between porosity and permeability for red and white dunes. Note separation of red and
 1003 white dunes.

1004 Fig. 11. SEM images of rock chips from Type 2 white sandstone. A) Authigenic assemblage of böhmite (bö),
 1005 kaolinite (kao), and calcite (calc). B) Kaolinite is totally replacing feldspar grains, and böhmite is coating quartz
 1006 and a relic feldspar in bottom right. C) Plagioclase being replaced by kaolinite and böhmite; this was the only
 1007 identifiable plagioclase grain encountered in the study. D) Close-up of kaolinite and böhmite authigenic
 1008 minerals. Q = quartz, plag = plagioclase, p = pore.

1009 Fig. 12. X-ray diffraction spectra for samples NG32 (red line, red sand, Type 1) and NG29 (blue line, white
 1010 sand, Type 2); important peaks are labelled. Plagioclase (albite and anorthite) peaks present in red sand are
 1011 absent in white sand, consistent with petrographical observations. White sand has peaks for kaolinite or chlorite
 1012 but red sand does not. Orthoclase peaks are also weakened in white sand. Interestingly no peak for böhmite was
 1013 produced despite its identification under SEM. kao= kaolinite, ch= chlorite, alb= albite, an= anorthite, or=
 1014 orthoclase.

1015 Fig. 13. Graph of major-element data in Appendix 2 normalized to NG52 values. A) NG32 red dune (red line)
 1016 and NG29 white dune (blue line). NG29 white has enriched CaO, and increased LOI. NG29 is leached of Na₂O

1017 and Fe₂O₃. B) NG26 white contact (blue line) and NG31 red contact (red line). CaO is enriched in both contact
 1018 samples, other elements except MnO show little variation, suggesting that both contacts (red and white dunes)
 1019 are the same.

1020 Fig. 14. Graphs for Dune A white, Dune B red, other white dunes, and other red dunes against distance below
 1021 hot contact. A) Authigenic quartz shows little correlation with distance because it is formed during burial, it
 1022 decreases where early compaction removed porosity during lava emplacement. B) Authigenic clay is generally
 1023 higher in the white sandstone but eogenetic clays in the red sandstone increase toward hot contact. C) Opaque
 1024 mineral abundance (grain rims and detrital) variability is high in red sandstone, the white sandstone opaque
 1025 mineral abundance increases toward hot contact, where eogenetic porosity loss prevented bleaching fluid
 1026 circulation. D) Authigenic calcite is generally higher in white dunes formed during circulation of bleaching
 1027 fluid, in red dunes calcite increases toward the contact due to volcano-eogenesis. Dune B red clearly shows a
 1028 decreasing calcite trend away from hot contact, whereas Dune A white calcite remains high and scattered with
 1029 increasing distance. See Table 3 for T-Test analysis of these data.

1030

1031 Fig. 15. A) $\delta^{13}\text{C}$ (PDB) plotted against $\delta^{18}\text{O}$ (PDB) for the four samples analyzed, plus two Type 3 contacts from
 1032 other formerly hot lava-sediment contacts. The calcite fields plotted for comparison are: (1) hydrothermally
 1033 affected graywacke, Horton et al., (2012); (2) carbonatite, Rollinson (1993); (3) hydrothermal calcite, Dias et
 1034 al., (2011); (4a, 4b) Entrada Fm hydrocarbon-related, Garden et al., (2001); (5) Navajo and Entrada Fms, Chan
 1035 et al., (2000); (6) Navajo Fm red cements, Beitler et al., (2005); (7) Permian playa lake, Platt et al., (1994); (8)
 1036 Namibia Karoo lava-related, Gierlowski-Kordesch et al., (2015); (9) Navajo Fm bleached cements, Beitler et al.,
 1037 (2005); (10) calcretes, Purvis and Wright (1991); (11) modern soil and groundwater carbonates, Europe, Candy
 1038 et al., (2012); (12) calcrete, Naylor et al., (1989); (13) South Africa calcretes, Solomons et al., (1978); (14)
 1039 Paraná. calcite geodes, Gilg et al, (2003). Type 2 and Type 3 diagenetic carbonates plot in two distinct
 1040 populations, with Type 3 red dune carbonate cements having more mantle-like $\delta^{13}\text{C}$ values. (B) Modelled calcite
 1041 $\delta^{18}\text{O}$ values in equilibrium with waters of different origins. Calculated meteoric and magmatic fields are shown
 1042 (using fractionation constants A = -3.39 and B = 2.78, O'Neil et al. 1969) as well as the expected meteoric
 1043 water, value for Namibia in the Cretaceous (132 Ma). $\delta^{18}\text{O}$ values of calcite from our analyses are plotted. NG
 1044 28, NG30, and NG34 are from white dunes (Type 2), NG31 is from Type 3 (lava-sediment contact) calcite.

1045 Fig. 16. Map of Dune C. Type 1 and Type 2 diagenesis is separated by a crosscutting N-S-trending dolerite dike.

1046 Fig. 17. Diagram showing the diagenetic evolution of the three sandstone types discussed. Type 3 diagenesis is
1047 labelled (3) and includes both red and white sandstones. The red (Type 1) sandstone is depicted by the red lines,
1048 and the white (Type 2) sandstone by the blue lines. After initial burial by lava the diagenetic pathways diverge
1049 and are labelled (1) for Type 1 diagenesis and (2) for Type 2 diagenesis.

1050 Fig. 18. Conceptual model of fluid flow through Dune Valley as controlled by igneous rocks. A) Dolerite dikes
1051 acting as barriers to horizontal fluid flow. B) Lateral fluid flow permitted through sandstone and basalt. C)
1052 Multidirectional flow permitted through sandstone. Diagram is not to scale.

1053 Appendix 1. Point-count data (500 points), and permeability data (nitrogen probe) presented for all red and
1054 white dunes sampled. *Repeat section.

1055 Appendix. 2. XRF Major element data for isolated-dune samples

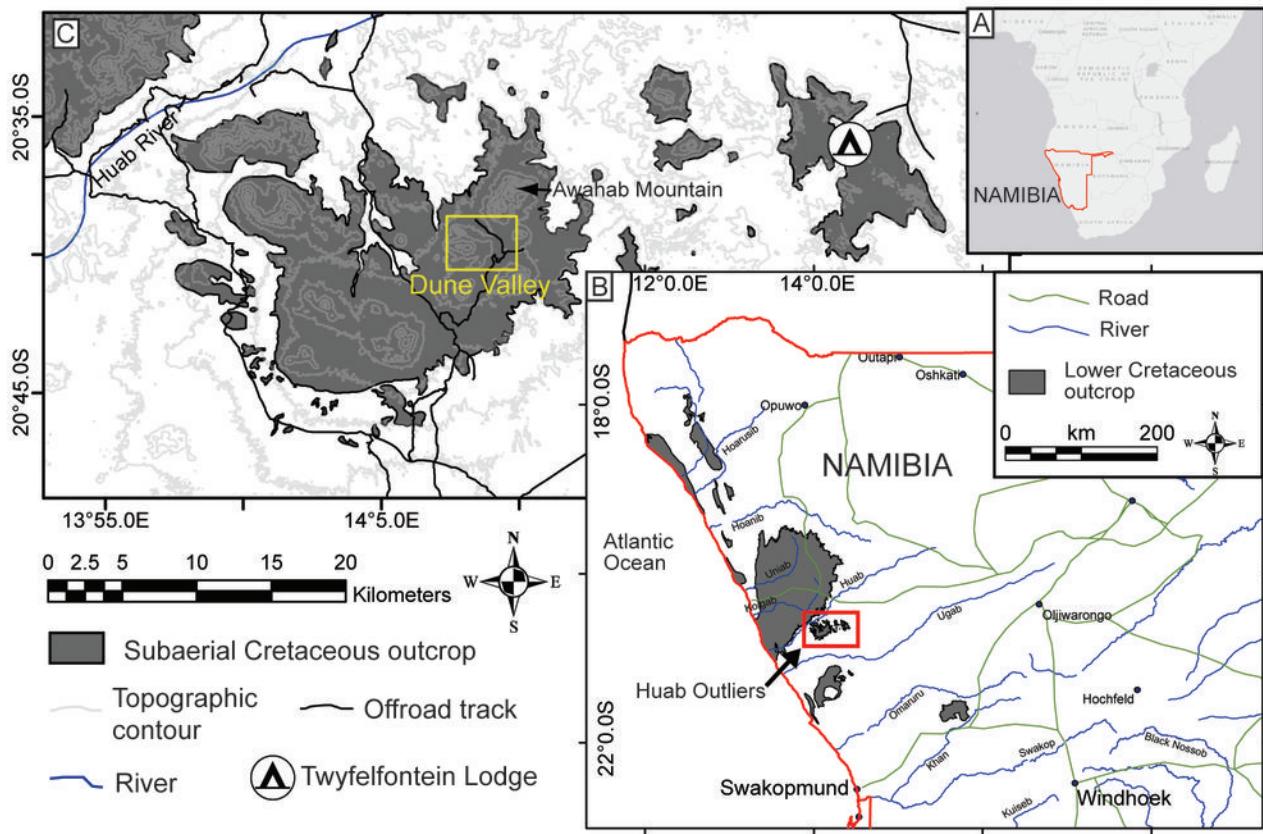
1056 Appendix. 3. Stable-isotope data for calcite in sandstone samples analyzed.

1057

1058

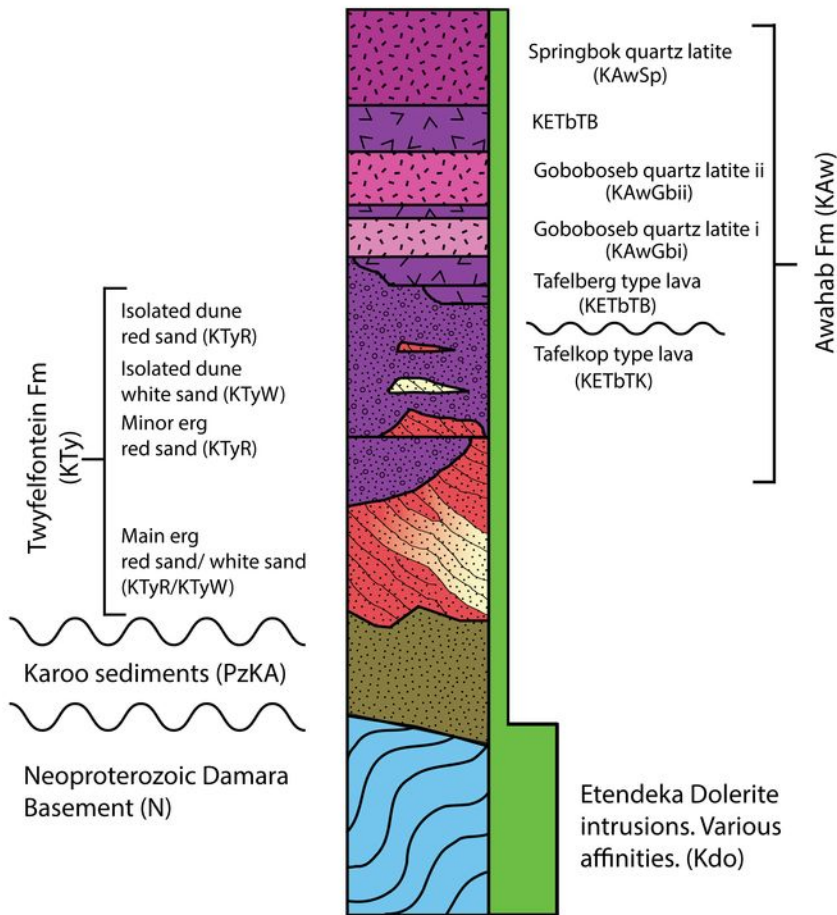
1059

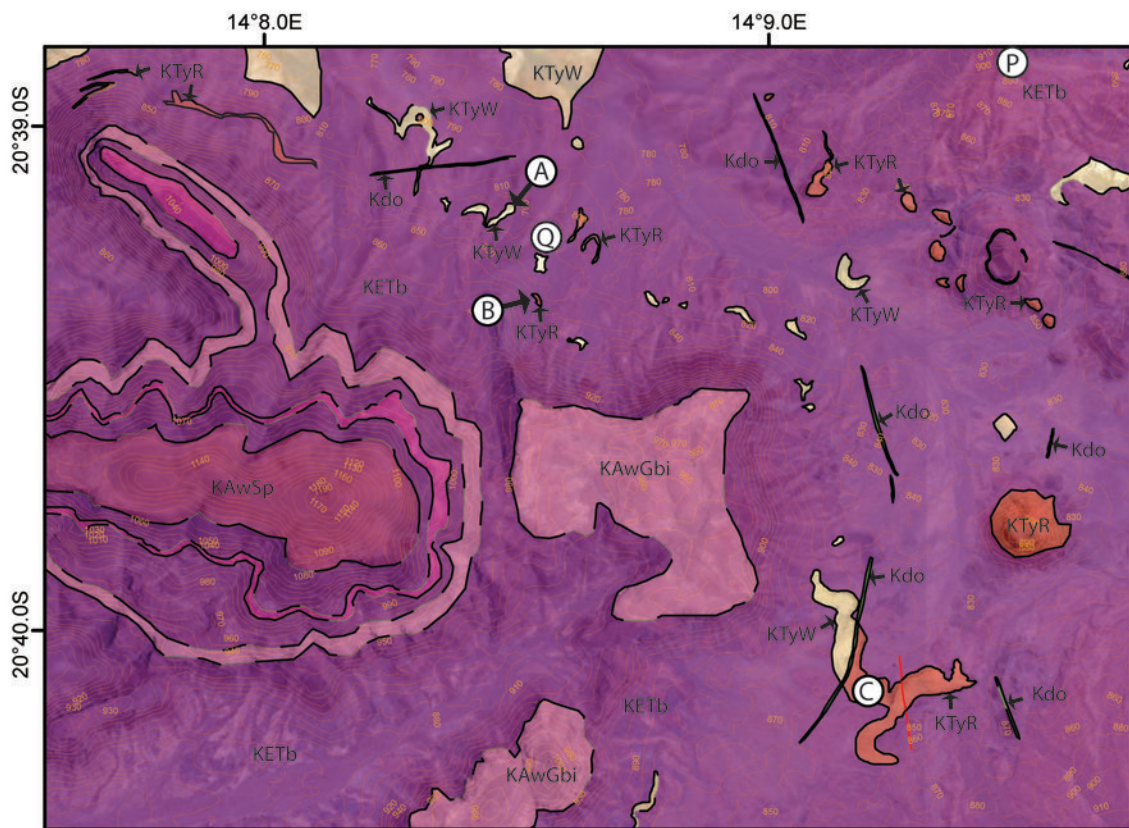
1060



Sedimentary

Igneous





Map Key

— Fault

KAwSp Springbok Quartz Latite

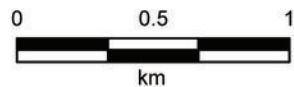
KAwGbi Goboboseb i Quartz Latite

KAwGbi Goboboseb ii Quartz Latite

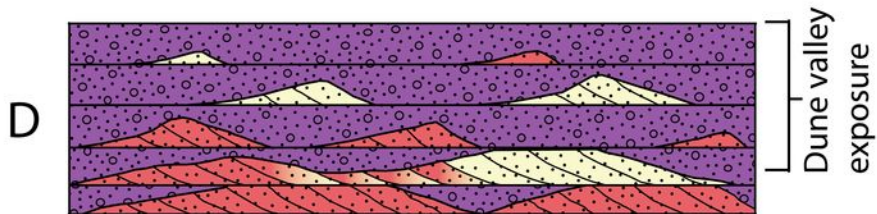
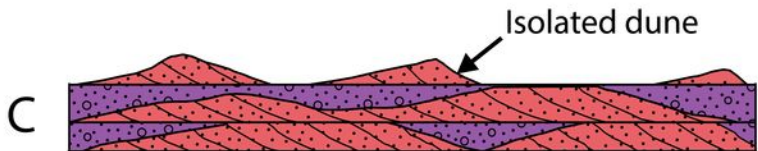
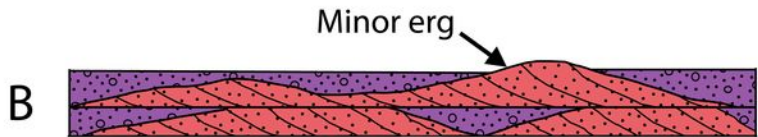
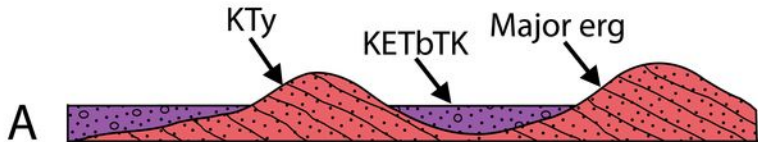
KETb Etendeka Basalts

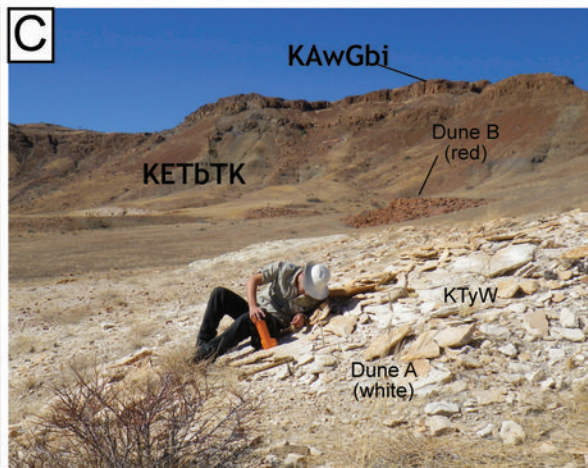
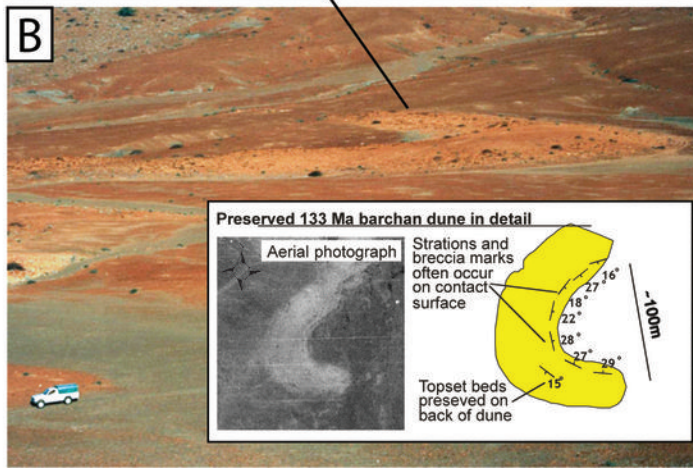
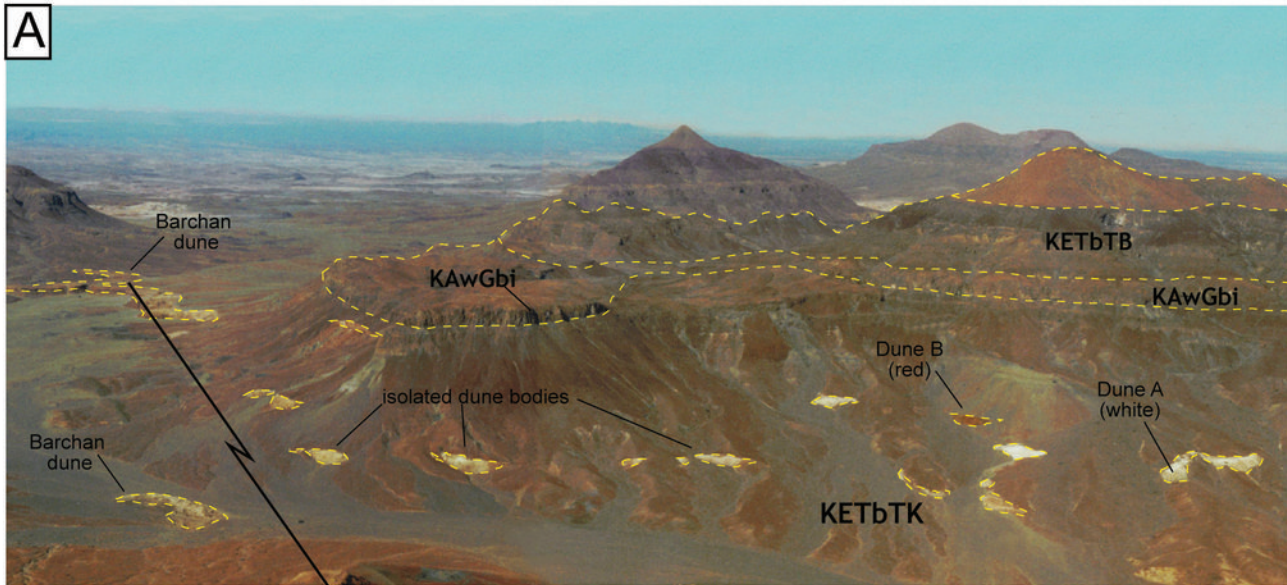
Red Twyfelfontein Fm **KTyR** **KTyW** White Twyfelfontein Fm

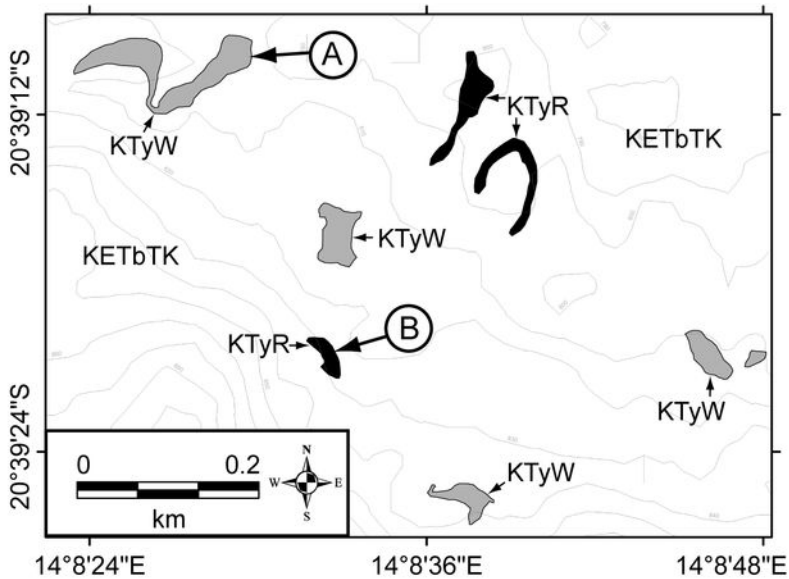
Kdo Basic igneous intrusion



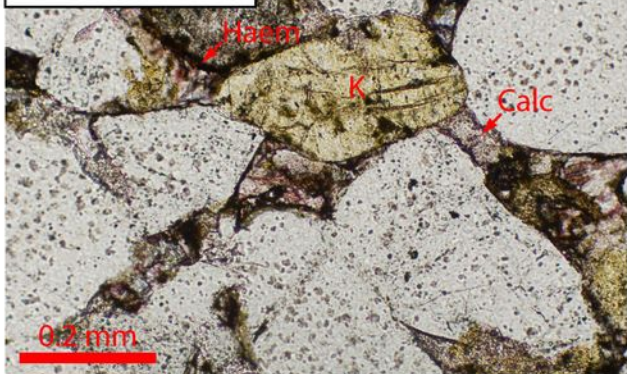
Map Datum: WGS 84
Contour interval 10 m



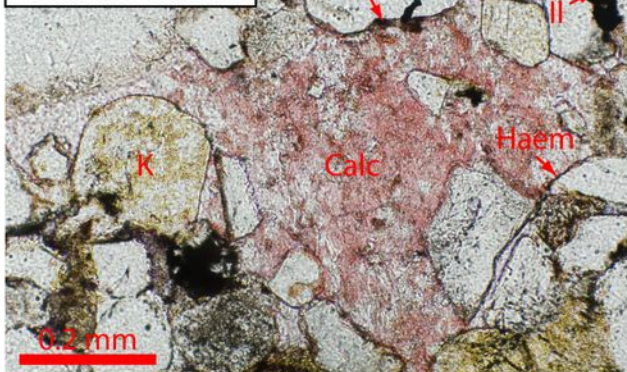




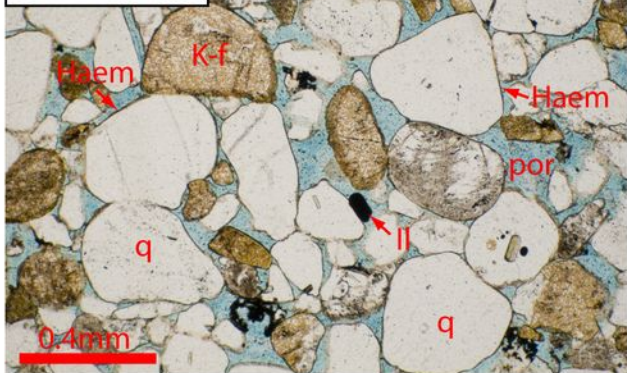
A. NG26 contact



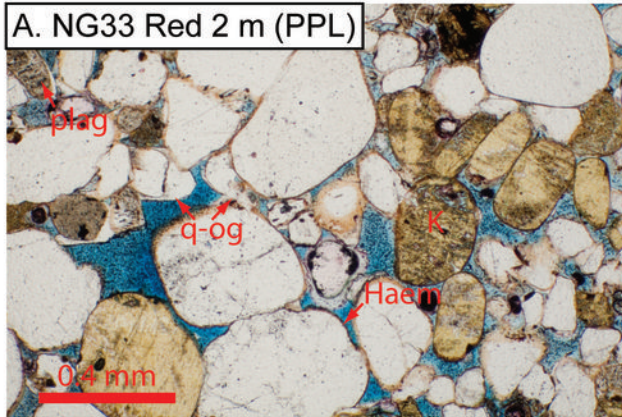
B. NG31 contact



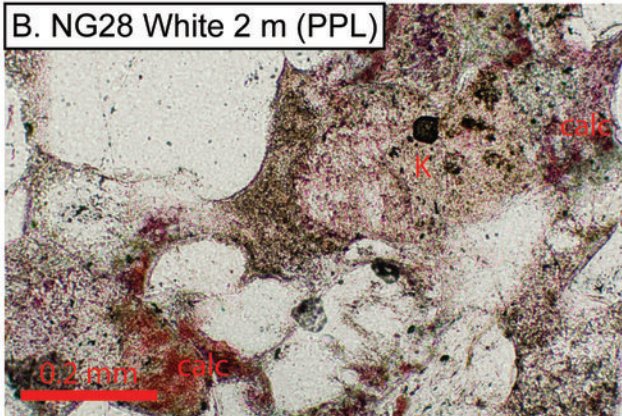
NG52 control



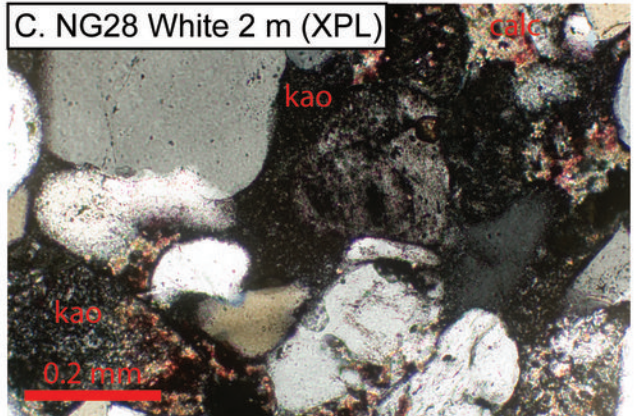
A. NG33 Red 2 m (PPL)



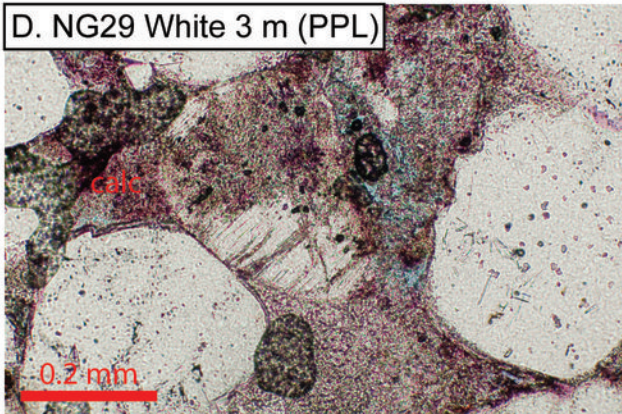
B. NG28 White 2 m (PPL)



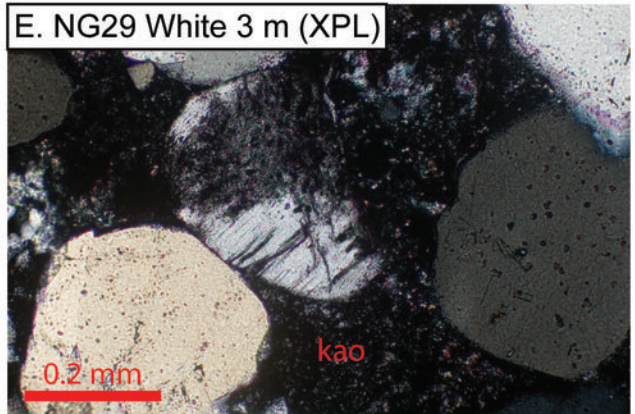
C. NG28 White 2 m (XPL)

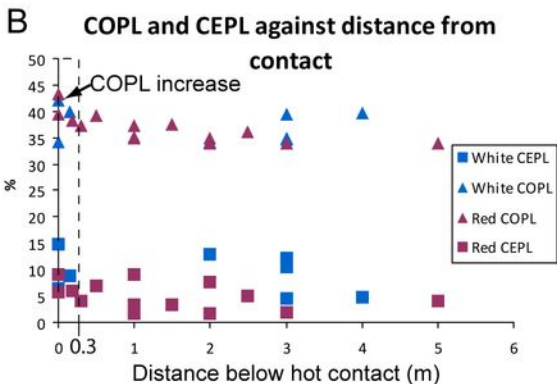
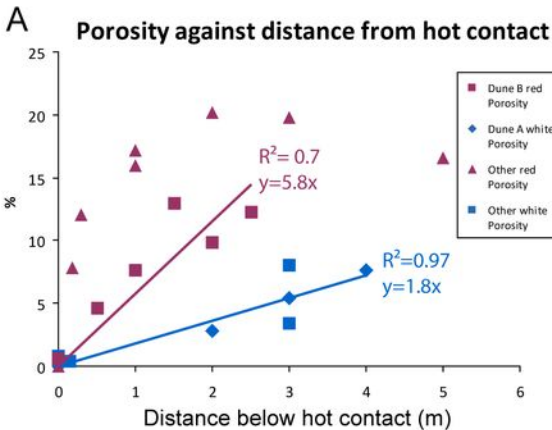


D. NG29 White 3 m (PPL)

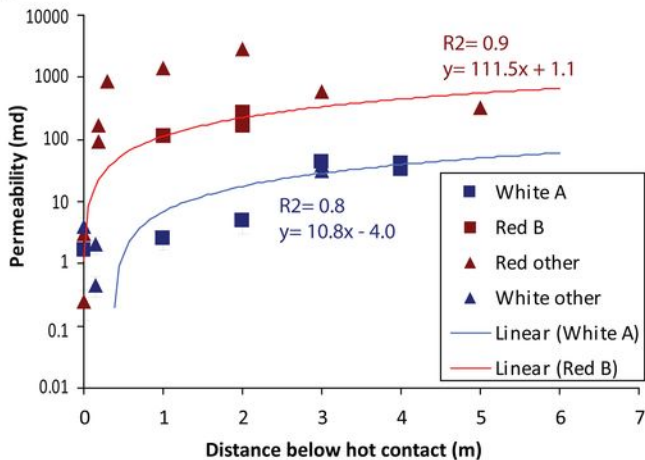


E. NG29 White 3 m (XPL)

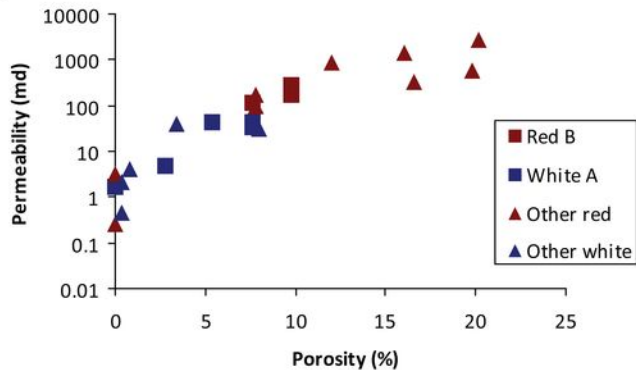


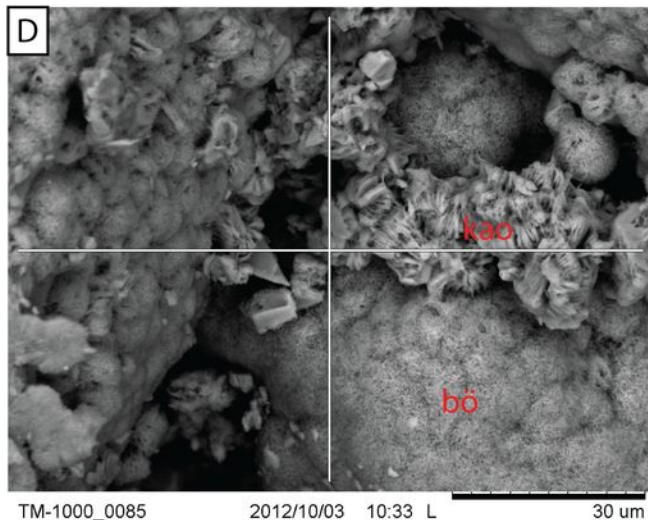
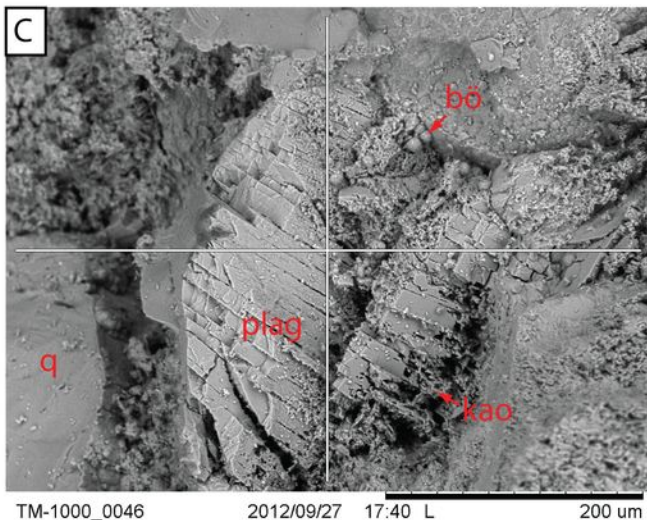
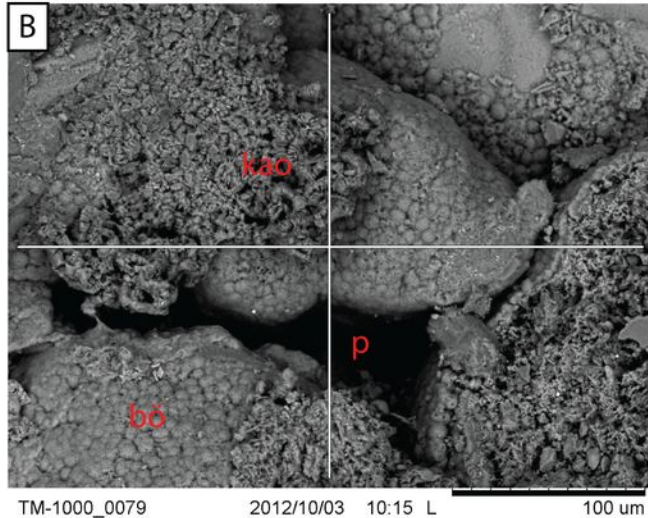
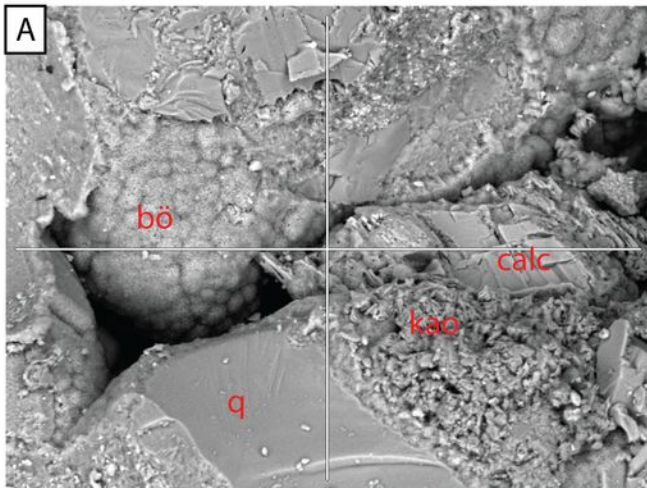


A

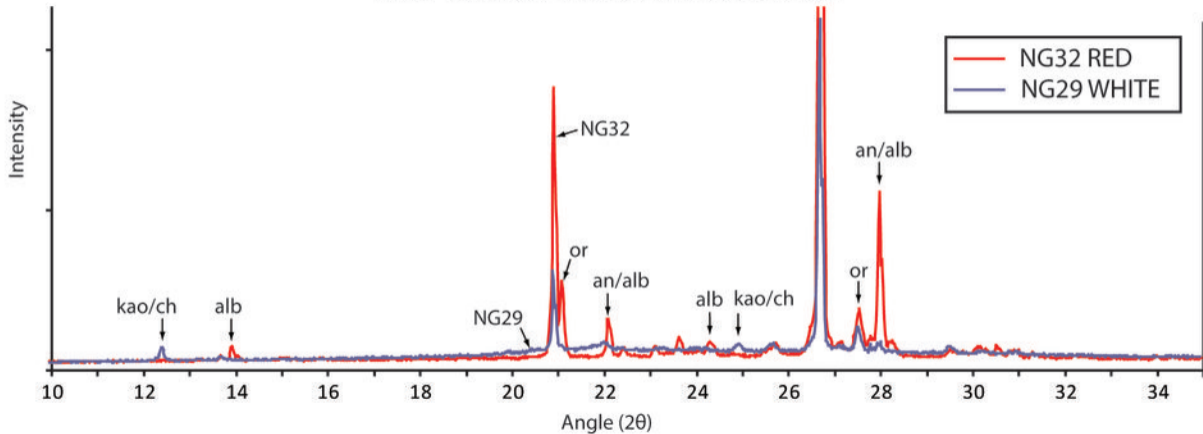


B

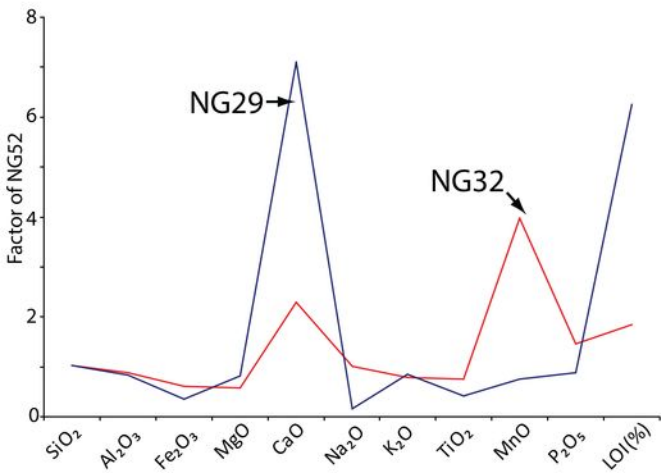




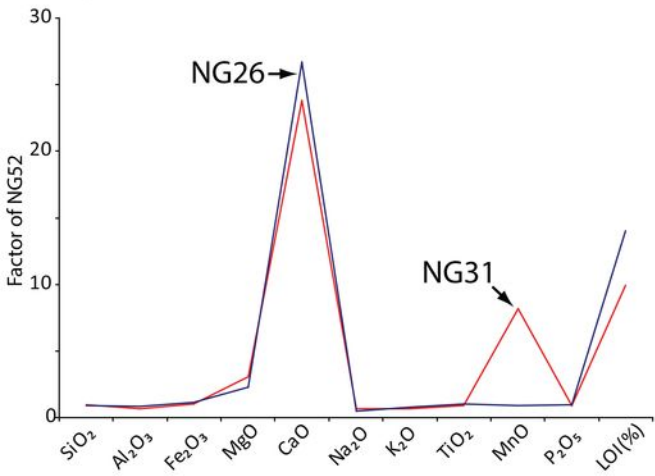
XRD- Dune A white and Dune B red



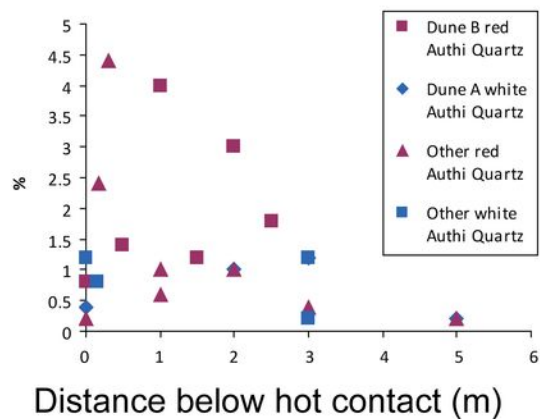
A: Type 1 (red) and Type 2 (white)



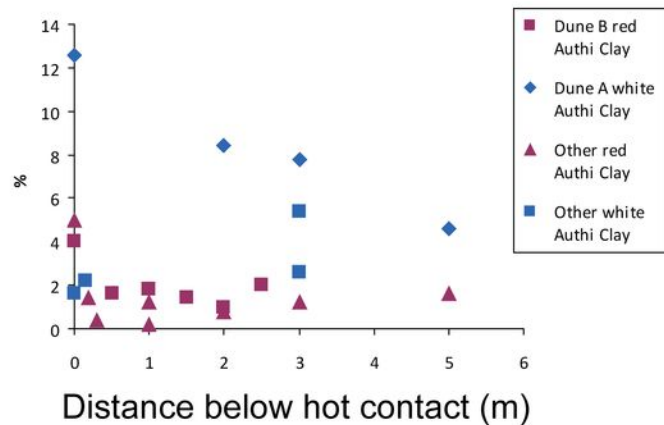
B: Type 3 (hot contact)



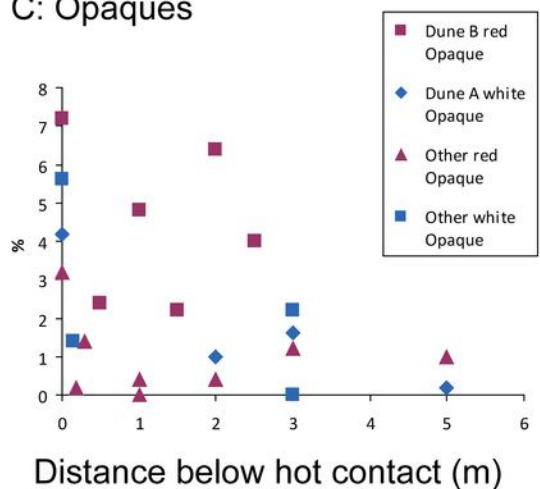
A: Authigenic Quartz



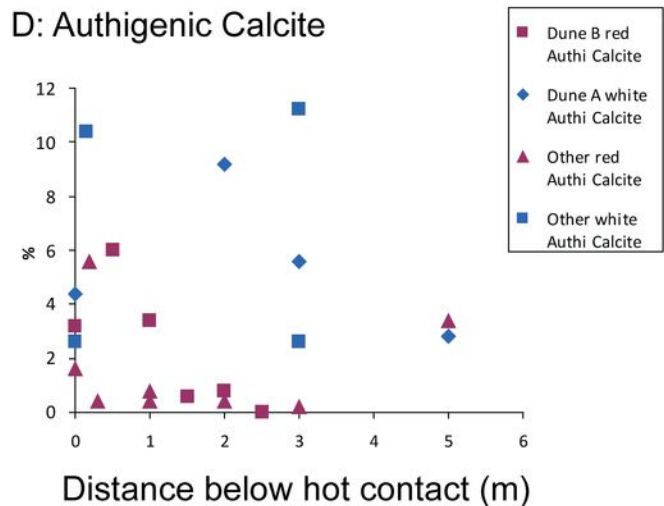
B: Authigenic Clay

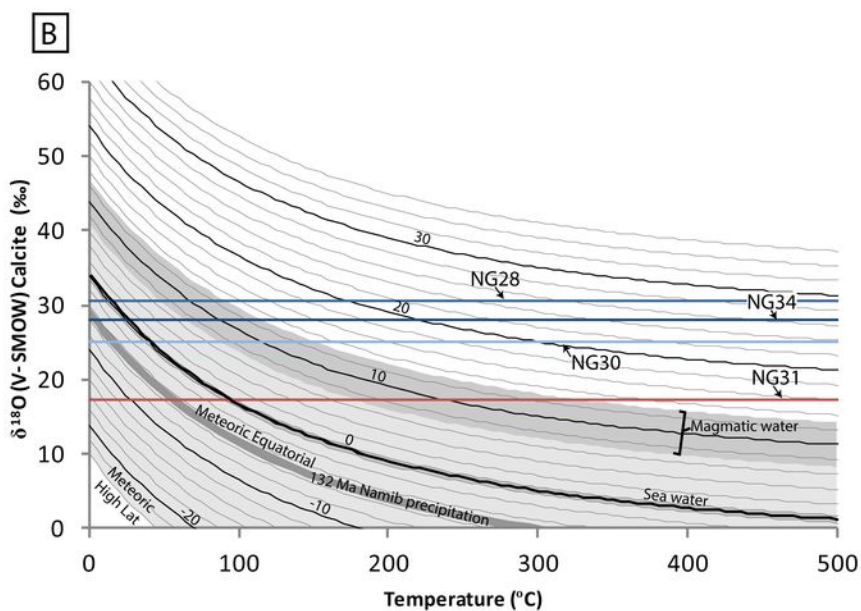
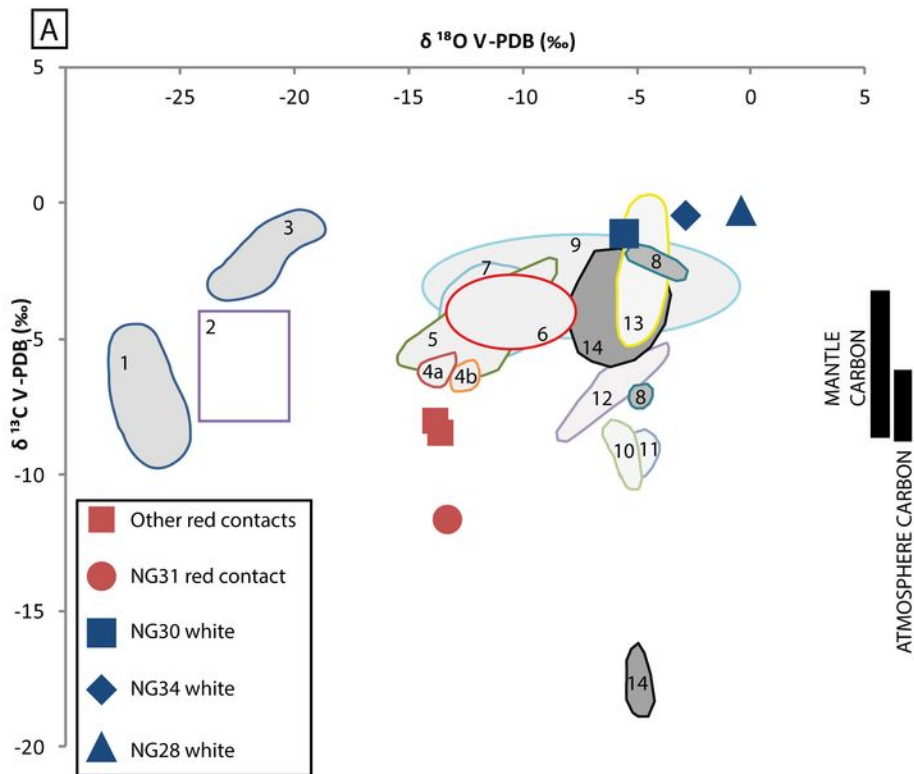


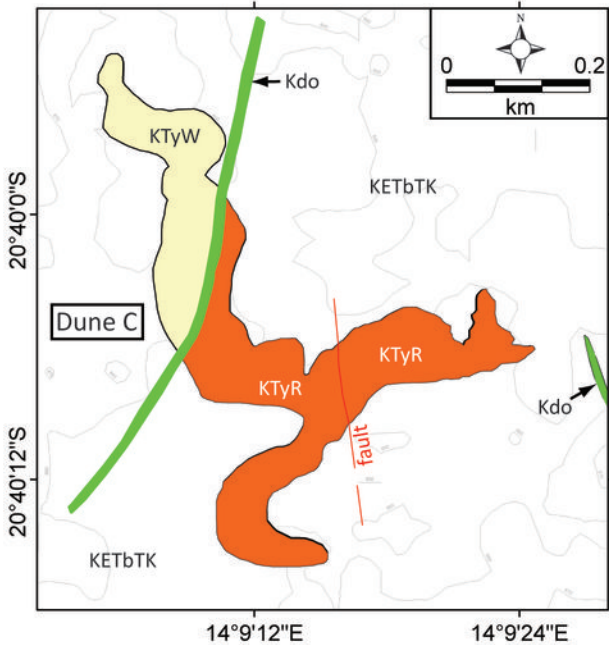
C: Opaques



D: Authigenic Calcite







Burial by lava &
During Etendeka Volcanism



Further Burial



Exhumation

COMPACTION BY LAVA

= ③

COMPACTION BY BURIAL

FELDSPAR DISSOLUTION

= ③

CALCITE CEMENT

= ③

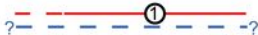
QUARTZ OVERGROWTHS

= ③

Fe OXIDE REDUCTION

KAOLINITE CEMENT

BÖHMITE CEMENT



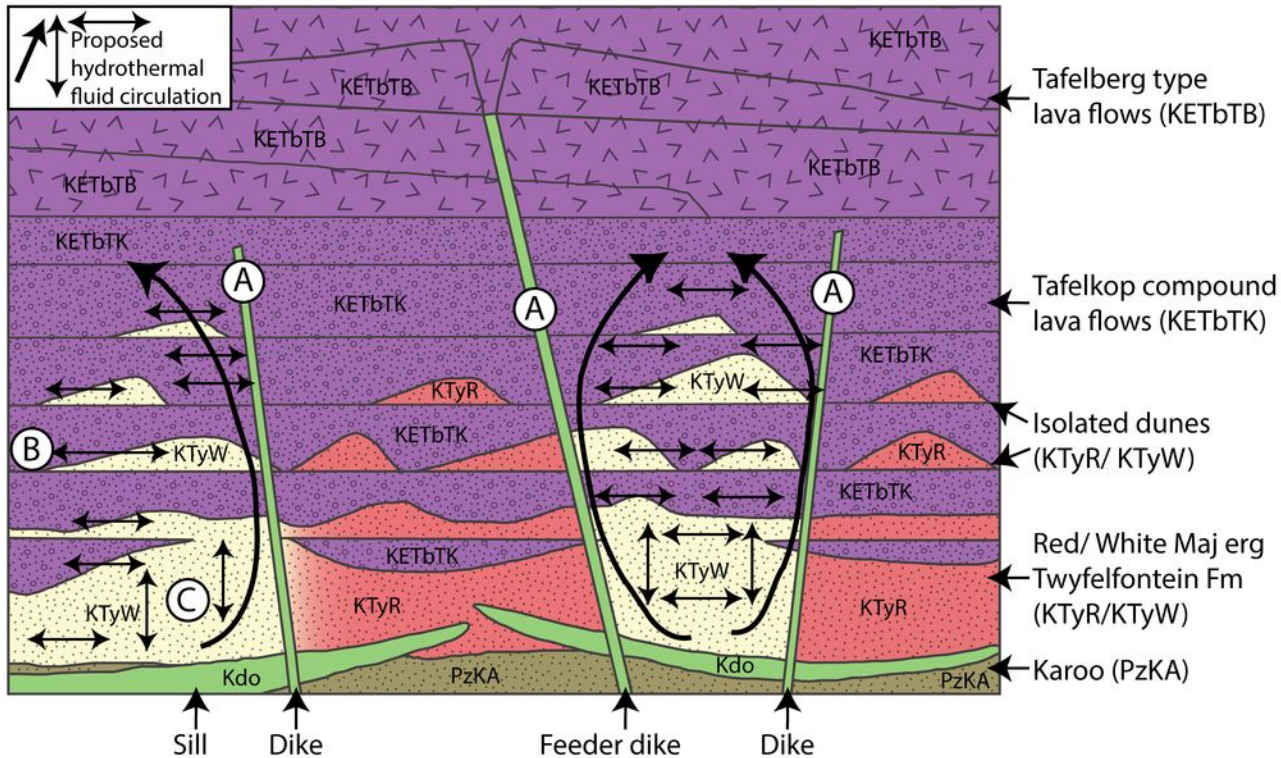


Table. 1. Average point-counting data for each “type” of diagenesis identified in this study. 500 points were counted for each sample.

Case	NG52 Red Control	Red (average)	White (average)	Contact (average)
Diagenesis	Type 1	Type 1	Type 2	Type 3
Distance below lava (m)	NA	2.0	2.7	0.2
Quartz %	55.2	50.0	60.4	54.9
K-Spar %	20.6	22.3	14.4	22.7
Plag %	7.4	6.5	4.1	5.3
Lithic %	1.2	0.6	0.6	0.8
Authi-Calcite %	0.0	0.8	5.9	4.7
Authi-Clay %	1.2	1.1	7.6	3.8
Authi-Q %	0.0	1.5	0.7	1.4
Authi-feldspar %	0.0	0.1	0.0	0.1
Porosity %	12.4	15.2	4.8	2.7
Opaque %	2.0	1.9	1.4	3.6
Fluorite %	0.0	0.2	0.1	0.0
Detrital Amphibole %	0.0	0.0	0.0	0.0
Zeolite %	0.0	0.0	0.1	0.0
Pmc	15.6	20.8	20.5	16.3
COPL %	39.6	35.6	35.7	38.9
CEPL %	7.5	3.6	10.3	8.4
ICOMPACT	0.8	0.9	0.8	0.8
Probe Permeability md	1747.4	1094.6	25.9	31.1

Table. 2. Petrological and mineralogical comparison of contact sediments at Dune A white and Dune B red.

Data type	Dune A white contact (NG 26)	Dune B red contact (NG31)	Control (NG52)
Petrographical	Highly compacted, feldspars altering to clays, pokilitic calcite cement	Highly compacted, feldspars altering to clays, pokilitic calcite cement	Compacted, low amount of alteration of detrital grains, pores and throats open. Cements absent.
XRD (authigenic in brackets)	Quartz, orthoclase, anorthite, albite, (calcite), (clinochlore or kaolinite)	Quartz, orthoclase, anorthite, albite, ilmenite, (calcite), (fluorite, weak), (clinochlore or kaolinite, weak)	Quartz, orthoclase, anorthite, albite, (iron minerals, weak peaks)

Table. 3. T-Test results of the point counting and permeability analysis of Type 1 red dunes and Type 2 white dunes. All parameters other than opaque minerals have a T-Test result showing that the phase counted is either statistically significantly different (95%) or highly statistically significantly different (99%). The opaque-mineral result supports the hypothesis that iron oxides are reprecipitated locally as nodules. Highly statistically significant results are appended with an asterisk.

Parameter	Probability different	Statistically significant
Porosity	0.001	YES*
Permeability	0.013	YES
Authigenic quartz	0.046	YES
Authigenic calcite	0.048	YES
Clay	<0.001	YES*
Opaque minerals	0.411	NO